

Mining Seasonal Temporal Patterns in Time Series

Van Long Ho*, Nguyen Ho*, Torben Bach Pedersen*
Department of Computer Science, Aalborg University, Denmark
*{vlh, ntth, tpb}@cs.aau.dk

Abstract—Very large time series are increasingly available from an ever wider range of IoT-enabled sensors, from which significant insights can be obtained through mining temporal patterns from them. A useful type of patterns found in many real-world applications exhibits periodic occurrences, and is thus called *seasonal temporal patterns* (STP). Compared to regular patterns, mining seasonal temporal patterns is more challenging since traditional measures such as *support* and *confidence* do not capture the seasonality characteristics. Further, the anti-monotonicity property does not hold for STPs, and thus, resulting in an exponential search space. This paper presents our Frequent Seasonal Temporal Pattern Mining from Time Series (FreqSTPFTS) solution providing: (1) The first solution for seasonal temporal pattern mining (STPM) from time series that can mine STP at different data granularities. (2) The STPM algorithm that uses efficient data structures and two pruning techniques to reduce the search space and speed up the mining process. (3) An approximate version of STPM that uses mutual information, a measure of data correlation, to prune unpromising time series from the search space. (4) An extensive experimental evaluation showing that STPM outperforms the baseline in runtime and memory consumption, and can scale to big datasets. The approximate STPM is up to an order of magnitude faster and less memory consuming than the baseline, while maintaining high accuracy.

I. INTRODUCTION

The widespread of IoT systems enables the collection of big time series from domains such as energy, transportation, climate, and healthcare. Mining such time series can discover hidden patterns and offer new insights into the application domains to support evidence-based decision making and planning. Often, pattern mining methods such as sequential pattern mining (SPM) [1], [2] and temporal pattern mining (TPM) [3], [4] are used to extract frequent (temporal) relations between events. In SPM, events occur in sequential order, whereas in TPM, events carry additional temporal information such as occurrence time, making relations between temporal events are more expressive and comprehensive. A useful type of temporal patterns found in many real-world applications are those that exhibit periodic occurrences. Such patterns occur concentrated within a particular time period, and then repeat that concentrated occurrence periodically. They are thus called *seasonal temporal patterns*. Here, the term *seasonal* indicates the periodic re-occurrence, while the term *temporal pattern* indicates patterns that are formed by the temporal relations between events, such as follows, contains, overlaps. Seasonal temporal patterns are useful in revealing seasonal information of temporal events and their relations. For example, in healthcare, health experts might be interested in finding seasonal diseases in a geographical location, as exemplified in Fig. 1

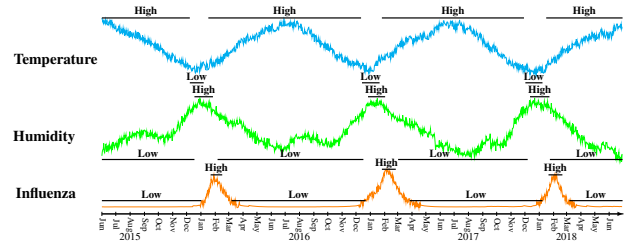


Fig. 1: Weather and Influenza time series

using the real-world data from Kawasaki, Japan between 2015 - 2018 [5], [6]. Here, a seasonal temporal pattern involving weather and epidemic events can be found: {Low Temperature overlaps High Humidity followed by High Influenza Cases}. This pattern occurs yearly and is concentrated in January, February. Detecting such seasonal diseases will support health experts in prevention and planning. In market analysis, knowing the periodic rise of certain stocks and their relations to other impact factors can be of interests for traders to plan better trading strategies. In marketing, identifying the order of search keywords that appear seasonally in the search engine can be useful to better understand customer needs and thereby improve the marketing plans.

Challenges. Although seasonal temporal patterns are useful, mining them is a challenging task for several reasons. First, the *support* measure used by TPM is not sufficient to mine seasonal patterns, since the traditional *support* represents the frequency of a pattern across the entire dataset, and thus, cannot capture the seasonality characteristic of seasonal patterns. Second, since temporal patterns are constructed based on temporal events, the complex relations between temporal events create an exponential and large search space of size $O(n^h 3^{h^2})$ (n is the number of events and h is the length of temporal patterns). Finally, since seasonal temporal patterns do not uphold the anti-monotonicity property, i.e., the non-empty subsets of a seasonal temporal pattern may not be seasonal, mining seasonal temporal patterns is more computationally expensive as the typical pruning technique based on anti-monotonicity property cannot be applied. This raises the need for an efficient seasonal temporal pattern mining approach with effective prunings to tackle the exponential search space. Existing work such as [7], [8] proposes solutions to mine seasonal itemsets. However, they do not consider the temporal aspect of items/ events, thus, addressing the exponential search space of seasonal temporal patterns is still an open problem.

Contributions. In the present paper, we present our Fre-

quent Seasonal Temporal Pattern Mining from Time Series (FreqSTPPTS) solution that addresses all the above challenges. Specifically, our key contributions are as follows. (1) We propose the first solution to mine *seasonal temporal patterns* from time series. Within the process, we introduce several measures to assess the seasonality characteristics, and use these to formally define the concept of *seasonal temporal patterns* in time series. The formulation allows to flexibly mine seasonal temporal patterns at different granularities. (2) Our Seasonal Temporal Pattern Mining (STPM) algorithm is efficient and has several important novelties. First, STPM employs efficient data structures, i.e., the hierarchical hash tables, to enable fast retrieval of candidate events and patterns during the mining process. Second, we define a new measure *maxSeason* that upholds the anti-monotonicity property, and design two efficient pruning techniques: Apriori-like pruning and transitivity pruning. (3) Based on mutual information, we propose a novel approximate version of STPM to prune unpromising time series and significantly reduce the search space, while maintaining highly accurate results. The approximate STPM can scale on big datasets, i.e., many time series and many sequences. (4) We perform extensive experimental evaluation on synthetic and real-world datasets from various domains showing that STPM outperforms the baseline in both runtime and memory usage. The approximate STPM achieves up to an order of magnitude speedup w.r.t. the baseline, while obtaining high accuracy compared to the exact STPM.

II. RELATED WORK

Finding seasonal patterns that represent temporal periodicity in time series is an important research topic, and has received substantial attention in the last decades. By considering seasonality as periodic occurrences, different techniques have been proposed to find periodic sub-sequences in time series data. Such techniques, first introduced by Han et al. in [9], [10], and later extended by [11]–[15], are called *motif* discovery techniques. However, since motifs are defined as similar time series sub-sequences, motif discovery can only find recurrent sub-sequences rather than periodic temporal patterns.

Another research direction in this area concerns periodic association rules [7], [8], [16]–[38]. Such techniques can identify seasonal associations between itemsets, for example, market-basket analysis to reveal the seasonal occurrence of the association {Glove \Rightarrow Winter Hat} during the winter season. To mine such seasonal itemset patterns in transactional databases, Tanbeer et al. in [16] proposed the PFP-growth algorithm using *minSup* and *maxPer* as seasonality measures. In their method, a tree structure called PF-tree is used as a compact representation of periodic frequent itemsets, with *maxPer* imposing the periodic constraint, and *minSup* imposing the frequency constraint on the pattern occurrences. Although PFP-growth can capture seasonality characteristic through the *maxPer* measure, the use of *minSup* means that it cannot identify rare seasonal patterns. Follow-up work such as [17], [18] improves different aspects of PFP-growth, for

example, Amphawan et al. [18] propose *period summary* to approximate the pattern periodicity to reduce the memory cost, Uday et al. [17] use the concept of *item-specific support* to address the rare pattern problem. Recently, Javed et al. [38] propose hashed occurrence vectors and Apriori-based approach to speed up periodic itemsets mining.

In a more recent work [7], Uday et al. propose the RP-growth algorithm to discover recurring itemset patterns in transactional databases. RP-growth uses an RP-tree to maintain frequent itemsets, and recursively mines the RP-tree to discover recurring ones. In their follow-up work, the same authors introduce several improvements of [7]. In [39], they propose the Periodic-Frequent Pattern-growth++ (PFP-growth++) algorithm that employs two new concepts, *local-periodicity* and *periodicity*, to capture locally optimal and globally optimal solutions of recurring patterns. This enables 2-phase pruning to improve the runtime efficiency. In [8], the authors extend PFP-growth++ to find periodic spatial patterns in spatio-temporal databases. In [37], PFP-growth++ is extended to find maximal periodic frequent patterns. In [40], they further improve PFP-growth++ to be memory efficient by proposing a concept called *period summary* to effectively summarize the temporal occurrence information of an itemset in a Periodic Summary-tree (PS-tree), and designing Periodic Summary Pattern Growth algorithm (PS-growth) to find all periodic-frequent itemset patterns from PS-tree. Nevertheless, all the mentioned work can only discover seasonal patterns between itemsets. To the best of our knowledge, no existing work addresses the seasonal temporal pattern mining that finds seasonal occurrences of temporal patterns. In Section VI, we adapt the state-of-the-art method for periodic itemset mining *PS-growth* to mine seasonal temporal patterns, and use it as an experimental baseline.

III. PRELIMINARIES

A. Time Granularity

Definition 3.1 (Time domain) A time domain \mathcal{T} consists of an ordered set of time instants that are isomorphic to the natural numbers. The time instants in \mathcal{T} have a time unit, presenting how they are measured.

Definition 3.2 (Time granularity) Given a time domain \mathcal{T} , a *time granularity* G is a *complete and non-overlapping equal partitioning* of \mathcal{T} , i.e., \mathcal{T} is divided into non-overlapping equal partitions. Each non-empty partition $G_i \in G$ is called a (time) *granule*. The position of a granule G_i in G , denoted as $p(G_i)$, is identified by counting the number of granules which appear before and up to (including) G_i . The *period* between two granules G_i and G_j in granularity G measures the time duration between G_i and G_j , and is computed as: $pr_{ij} = |p(G_i) - p(G_j)|$, where $p(G_i)$ and $p(G_j)$ are the positions of G_i and G_j , respectively.

As an example, consider a time domain \mathcal{T} consisting of an ordered set of minutes. The time instants $minute_1$, $minute_2$, etc. are isomorphically mapped to the natural numbers, and are measured in the *Minute* time unit. Here, \mathcal{T} can have different time granularities such as Minute, 5-Minutes, or even Hour,

TABLE I: Frequently Used Notations

Notation	Description
\mathcal{T}, \mathcal{H}	time domain \mathcal{T} and time granularity hierarchy \mathcal{H}
$p(G_i)$	the position of the granule G_i
$G \trianglelefteq_m H$	granularity G is m -Finer than granularity H
X, X_S	time series X and symbolic time series X_S
$E_{\triangleright e}$	temporal event E has an event instance e
$g: X_S \rightarrow_m H$	sequence mapping from X_S to granularity H
$Seq_i = \langle e_1, \dots, e_n \rangle$	a temporal sequence of n event instances
$\mathcal{D}_{\text{SYB}}, \mathcal{D}_{\text{SEQ}}$	symbolic database and temporal sequence database
H_i^E, H_i^P	event E (pattern P) occurs at granularity H_i
$\text{SUP}^E, \text{SUP}^P$	support set of event E (pattern P)
NearSUP_i^P	near support set i of pattern P
$\text{den}(\text{NearSUP}_i^P)$	density of the near support set
$\text{dist}(\text{NearSUP}_i^P, \text{NearSUP}_j^P)$	distance between two near support sets
$\text{seasons}(P)$	number of seasons of pattern P

Day, Year. The position of granule Minute₂ in the Minute granularity is $p(\text{Minute}_2) = 2$. The period between the Minute₁ and Minute₆ granules is: $|p(\text{Minute}_6) - p(\text{Minute}_1)| = 5$, indicating that the time duration between them is 5 minutes. We note that the period is only defined between granules of the same granularity.

Definition 3.3 (Finer time granularity) A time granularity G is *finer* than a time granularity H if and only if for every granule $H_j \in H$, there exists m adjacent granules $G_{i+1}, \dots, G_{i+m} \in G$ such that $H_j = G_{i+1} \cup \dots \cup G_{i+m}$ where $m \geq 1$. We call G is m -Finer than H , denoted as $G \trianglelefteq_m H$.

In the previous example, we have the Minute granularity is 60-Finer than the Hour granularity.

Definition 3.4 (Time granularity hierarchy) Given a time domain \mathcal{T} , the different time granularities of \mathcal{T} form a *time granularity hierarchy* \mathcal{H} where each level in \mathcal{H} represents one specific granularity, with the lower levels in the hierarchy having finer granularity than the higher levels.

Fig. 2 shows an example of the time granularity hierarchy. Here, to be consistent with examples in the following sections, we assume granularity G is 5-Minutes and is the finest, whereas granularity H is 15-Minutes and $G \trianglelefteq_3 H$.

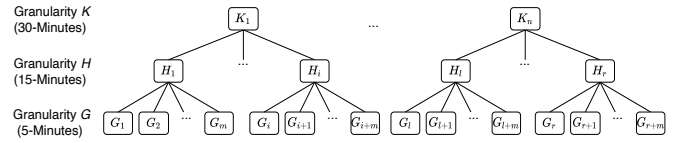
B. Symbolic Representation of Time Series

Consider the time domain \mathcal{T} . Let \mathcal{H} be the time granularity hierarchy of \mathcal{T} , and G be the finest granularity in \mathcal{H} .

Definition 3.5 (Time series) A *time series* $X = x_1, x_2, \dots, x_n$ in the time domain \mathcal{T} is a sequence of data values that measure the same phenomenon during an observation time period in \mathcal{T} , and are chronologically ordered. We say that X has granularity G if X is sampled at every time instant t_i in \mathcal{T} .

A *symbolic time series* X_S of X encodes the raw values of X into a sequence of symbols using a mapping function $f: X \rightarrow \Sigma_X$ that maps each value $x_i \in X$ into a symbol $\omega \in \Sigma_X$. The finite set of permitted symbols used to encode X is called the *symbol alphabet* of X , denoted as Σ_X . Since the mapping function f performs the 1-to-1 mapping from X to X_S , X_S has the same granularity G as X .

For example, let $X = 1.82, 1.25, 0.46, 0.0$ be a time series representing the energy usage of an electrical device recorded every 5 minutes. By using $\Sigma_X = \{1, 0\}$ (1: ON, 0: OFF), we obtain $X_S = 1, 1, 1, 0$. The mapping function f can be defined using time series representation techniques such as SAX [41].


 Fig. 2: Time granularity hierarchy \mathcal{H}

Definition 3.6 (Symbolic database) Given a set of time series $\mathcal{X} = \{X_1, \dots, X_n\}$, the set of symbolic representations of the time series in \mathcal{X} forms a *symbolic database* \mathcal{D}_{SYB} .

Table II shows an example of the symbolic database \mathcal{D}_{SYB} using $\Sigma = \{0, 1\}$. There are 5 time series: $\{C, D, F, M, N\}$ (C: Cooker, D: Dish Washer, F: Food Processor, M: Microwave, N: Nespresso Coffee) representing the energy usage of electrical devices at 5-Minutes granularity.

C. Temporal Event and Temporal Relation

Definition 3.7 (Temporal event) Consider a symbolic time series X_S . A *temporal event* E in X_S is a tuple $E = (\omega, T)$ where $\omega \in \Sigma_X$ is a symbol, and $T = \{[t_{s_i}, t_{e_i}]\}$ is the set of time intervals during which X_S has the value ω . Each time interval has t_{s_i} as the start time, and t_{e_i} as the end time.

Instance of a temporal event: The tuple $e = (\omega, [t_{s_i}, t_{e_i}])$ is called an *instance* of the temporal event $E = (\omega, T)$, representing a single occurrence of E during $[t_{s_i}, t_{e_i}]$. We use the notation $E_{\triangleright e}$ to denote that the event E has an instance e .

Consider the symbolic time series C in Table II. Then $E = (C:1, \{[G_1, G_2], [G_4, G_4], [G_7, G_8], [G_{19}, G_{24}], [G_{31}, G_{31}], [G_{34}, G_{35}], [G_{40}, G_{41}]\})$ is an event of C, representing the time intervals during which C is associated with the symbol 1. The tuple $(C:1, [G_1, G_2])$ is an instance of E . Note that for simplicity, we use the granules to represent the start and end times of the time intervals, as we can trace back the timestamp associated to each granule.

Relations between temporal events: Let E_i and E_j be two temporal events, and $e_i = (\omega_i, [t_{s_i}, t_{e_i}])$, $e_j = (\omega_j, [t_{s_j}, t_{e_j}])$ be their corresponding instances. We rely on the popular Allens relation model [42] to define 3 basic temporal relations: *Follows*, *Contains*, *Overlaps* between E_i and E_j through e_i and e_j . We avoid the exact time mapping problem in Allens relations by adding a tolerance *buffer* ϵ to the relation's endpoints, while ensuring the relations are *mutually exclusive* (proof in the technical report [43]). Table III illustrates the three relations and their conditions, with $\epsilon \geq 0$ being the buffer size, and d_o representing the minimal overlapping duration between two event instances in an Overlaps relation.

Definition 3.8 (Temporal pattern) Let $\mathfrak{R} = \{\text{Follows}, \text{Contains}, \text{Overlaps}\}$ be the set of temporal relations. A *temporal pattern* $P = \langle (r_{12}, E_1, E_2), \dots, (r_{(n-1)n}, E_{n-1}, E_n) \rangle$ is a list of triples (r_{ij}, E_i, E_j) , each representing a relation $r_{ij} \in \mathfrak{R}$ between two events E_i and E_j .

Note that each relation r_{ij} is formed using the specific instances of E_i and E_j . A temporal pattern of n events is called an n -event pattern. We use $E_i \in P$ to denote that the event E_i occurs in P , and $P_1 \subseteq P$ to say that a pattern P_1 is a sub-pattern of P . An example temporal pattern is shown in

TABLE II: A Symbolic Database \mathcal{D}_{SYB} (G: 5-Minutes granularity)

Granules in G	G ₁	G ₂	G ₃	G ₄	G ₅	G ₆	G ₇	G ₈	G ₉	G ₁₀	G ₁₁	G ₁₂	G ₁₃	G ₁₄	G ₁₅	G ₁₆	G ₁₇	G ₁₈	G ₁₉	G ₂₀	G ₂₁	G ₂₂	G ₂₃	G ₂₄	G ₂₅	G ₂₆	G ₂₇	G ₂₈	G ₂₉	G ₃₀	G ₃₁	G ₃₂	G ₃₃	G ₃₄	G ₃₅	G ₃₆	G ₃₇	G ₃₈	G ₃₉	G ₄₀	G ₄₁	G ₄₂				
Position	1	2	3	4	5	6	7	8	9	10	11	12	13	14	15	16	17	18	19	20	21	22	23	24	25	26	27	28	29	30	31	32	33	34	35	36	37	38	39	40	41	42				
Time series	C	1	1	0	1	0	0	1	1	0	0	0	0	0	0	0	0	0	1	1	1	1	1	1	0	0	0	0	0	0	0	1	0	0	1	1	0	0	0	0	1	1	0			
	D	1	0	0	1	0	0	1	1	0	1	1	0	0	0	0	0	0	1	1	1	1	1	1	0	0	0	0	0	0	1	0	0	1	0	0	1	1	0	1	1	0	1	1	0	
	F	0	0	1	0	1	1	0	0	1	0	0	1	1	1	1	0	0	0	0	0	0	0	0	0	0	1	1	1	1	1	1	0	0	1	0	0	1	0	1	0	0	1	0	0	1
	M	1	1	1	1	0	0	1	1	1	1	1	0	1	1	1	1	1	1	0	0	0	0	1	1	1	1	1	1	1	1	1	1	1	0	0	0	1	1	1	1	0	0	0	0	
N	1	1	0	1	1	1	1	1	1	1	0	1	1	1	1	1	1	1	0	0	0	0	0	0	0	1	1	1	1	1	1	1	1	1	1	1	1	1	1	1	1	1	0	0	0	

TABLE III: Temporal Relations between Events

Follows: $E_{i \pm e_i} \succ E_{j \pm e_j}$	$t_{s_i} + e_i < t_{s_j}$	$t_{s_i} + e_i \leq t_{s_j}$
Contains: $E_{i \pm e_i} \supseteq E_{j \pm e_j}$	$t_{s_i} \leq t_{s_j} \wedge t_{s_i} + e_i \leq t_{s_j} + e_j$	$t_{s_i} \leq t_{s_j} \wedge t_{s_i} + e_i < t_{s_j} + e_j$
	$(t_{s_i} < t_{s_j}) \wedge (t_{s_i} + e_i < t_{s_j}) \wedge (t_{s_j} < t_{s_i} + e_j)$	$(t_{s_i} < t_{s_j}) \wedge (t_{s_i} + e_i < t_{s_j}) \wedge (t_{s_j} < t_{s_i} + e_j)$
Overlaps: $E_{i \pm e_i} \cap E_{j \pm e_j}$	$(t_{s_i} < t_{s_j}) \wedge (t_{s_i} + e_i < t_{s_j}) \wedge (t_{s_j} < t_{s_i} + e_j)$	$(t_{s_i} < t_{s_j}) \wedge (t_{s_i} + e_i < t_{s_j}) \wedge (t_{s_j} < t_{s_i} + e_j)$

 TABLE IV: A Temporal Sequence Database \mathcal{D}_{SEQ} (H: 15-Minutes granularity)

Granules	Position	Temporal sequences
$H_1 = \{G_1, G_2, G_3\}$	1	(C:1,[G ₁ ,G ₂]), (C:0,[G ₃ ,G ₃]), (D:1,[G ₁ ,G ₁]), (D:0,[G ₂ ,G ₃]), (F:0,[G ₁ ,G ₂]), (F:1,[G ₃ ,G ₃]), (M:1,[G ₁ ,G ₃]), (N:1,[G ₁ ,G ₂]), (N:0,[G ₃ ,G ₃])
$H_2 = \{G_4, G_5, G_6\}$	2	(C:1,[G ₄ ,G ₄]), (C:0,[G ₅ ,G ₆]), (D:1,[G ₄ ,G ₄]), (D:0,[G ₅ ,G ₆]), (F:0,[G ₄ ,G ₄]), (F:1,[G ₅ ,G ₆]), (M:1,[G ₄ ,G ₄]), (M:0,[G ₅ ,G ₆]), (N:1,[G ₄ ,G ₆]), (F:1,[G ₅ ,G ₆]), (M:1,[G ₇ ,G ₈]), (D:1,[G ₇ ,G ₈]), (D:0,[G ₉ ,G ₉]), (F:0,[G ₇ ,G ₈]), (F:1,[G ₉ ,G ₉]), (M:1,[G ₇ ,G ₉]), (N:1,[G ₇ ,G ₉])
$H_3 = \{G_7, G_8, G_9\}$	3	(C:1,[G ₇ ,G ₈]), (C:0,[G ₉ ,G ₉]), (D:1,[G ₇ ,G ₈]), (D:0,[G ₉ ,G ₉]), (F:0,[G ₇ ,G ₈]), (F:1,[G ₉ ,G ₉]), (M:1,[G ₇ ,G ₉]), (N:1,[G ₇ ,G ₉])
$H_4 = \{G_{10}, G_{11}, G_{12}\}$	4	(C:0,[G ₁₀ ,G ₁₂]), (D:1,[G ₁₀ ,G ₁₁]), (D:0,[G ₁₂ ,G ₁₂]), (F:0,[G ₁₀ ,G ₁₁]), (F:1,[G ₁₂ ,G ₁₂]), (M:1,[G ₁₀ ,G ₁₁]), (M:0,[G ₁₂ ,G ₁₂]), (N:1,[G ₁₀ ,G ₁₁]), (N:0,[G ₁₂ ,G ₁₂])
$H_5 = \{G_{13}, G_{14}, G_{15}\}$	5	(C:0,[G ₁₃ ,G ₁₅]), (D:0,[G ₁₃ ,G ₁₅]), (F:1,[G ₁₃ ,G ₁₅]), (M:1,[G ₁₃ ,G ₁₅]), (N:1,[G ₁₃ ,G ₁₅])
$H_6 = \{G_{16}, G_{17}, G_{18}\}$	6	(C:0,[G ₁₆ ,G ₁₈]), (D:0,[G ₁₆ ,G ₁₈]), (F:0,[G ₁₆ ,G ₁₈]), (M:1,[G ₁₆ ,G ₁₈]), (N:1,[G ₁₆ ,G ₁₈])
$H_7 = \{G_{19}, G_{20}, G_{21}\}$	7	(C:1,[G ₁₉ ,G ₂₁]), (D:1,[G ₁₉ ,G ₂₁]), (F:0,[G ₁₉ ,G ₂₁]), (M:0,[G ₁₉ ,G ₂₁]), (N:0,[G ₁₉ ,G ₂₁])
$H_8 = \{G_{22}, G_{23}, G_{24}\}$	8	(C:1,[G ₂₂ ,G ₂₄]), (D:1,[G ₂₂ ,G ₂₄]), (F:0,[G ₂₂ ,G ₂₄]), (M:1,[G ₂₂ ,G ₂₄]), (N:0,[G ₂₂ ,G ₂₄])
$H_9 = \{G_{25}, G_{26}, G_{27}\}$	9	(C:0,[G ₂₅ ,G ₂₇]), (D:0,[G ₂₅ ,G ₂₇]), (F:1,[G ₂₅ ,G ₂₇]), (M:1,[G ₂₅ ,G ₂₇]), (N:1,[G ₂₅ ,G ₂₇])
$H_{10} = \{G_{28}, G_{29}, G_{30}\}$	10	(C:0,[G ₂₈ ,G ₃₀]), (D:0,[G ₂₈ ,G ₃₀]), (F:1,[G ₂₈ ,G ₃₀]), (M:1,[G ₂₈ ,G ₃₀]), (N:1,[G ₂₈ ,G ₃₀])
$H_{11} = \{G_{31}, G_{32}, G_{33}\}$	11	(C:1,[G ₃₁ ,G ₃₁]), (C:0,[G ₃₂ ,G ₃₃]), (D:1,[G ₃₁ ,G ₃₁]), (D:0,[G ₃₂ ,G ₃₃]), (F:0,[G ₃₁ ,G ₃₂]), (F:1,[G ₃₃ ,G ₃₃]), (M:1,[G ₃₁ ,G ₃₃]), (N:1,[G ₃₁ ,G ₃₃])
$H_{12} = \{G_{34}, G_{35}, G_{36}\}$	12	(C:1,[G ₃₄ ,G ₃₅]), (C:0,[G ₃₆ ,G ₃₆]), (D:1,[G ₃₄ ,G ₃₄]), (D:0,[G ₃₅ ,G ₃₆]), (F:0,[G ₃₄ ,G ₃₅]), (F:1,[G ₃₆ ,G ₃₆]), (M:0,[G ₃₄ ,G ₃₆]), (N:1,[G ₃₄ ,G ₃₆])
$H_{13} = \{G_{37}, G_{38}, G_{39}\}$	13	(C:0,[G ₃₇ ,G ₃₉]), (D:1,[G ₃₇ ,G ₃₈]), (D:0,[G ₃₉ ,G ₃₉]), (F:0,[G ₃₇ ,G ₃₈]), (F:1,[G ₃₉ ,G ₃₉]), (M:1,[G ₃₇ ,G ₃₉]), (N:1,[G ₃₇ ,G ₃₉])
$H_{14} = \{G_{40}, G_{41}, G_{42}\}$	14	(C:1,[G ₄₀ ,G ₄₁]), (C:0,[G ₄₂ ,G ₄₂]), (D:1,[G ₄₀ ,G ₄₁]), (D:0,[G ₄₂ ,G ₄₂]), (F:0,[G ₄₀ ,G ₄₁]), (F:1,[G ₄₂ ,G ₄₂]), (M:0,[G ₄₀ ,G ₄₂]), (N:0,[G ₄₀ ,G ₄₂])

Fig. 1: $P = \langle \langle \text{Overlaps, Low Temperature, High Humidity} \rangle, \langle \text{Follows, Low Temperature, High Influenza Cases} \rangle, \langle \text{Follows, High Humidity, High Influenza Cases} \rangle \rangle$. Here, P is a 3-event pattern, containing pairwise temporal relations between Low Temperature, High Humidity, and High Influenza Cases.

D. Temporal Sequence Database

Definition 3.9 (Sequence mapping) Consider a symbolic time series X_S of granularity G . Let H be a granularity in \mathcal{H} such that $G \trianglelefteq_m H$. A sequence mapping $g: X_S \rightarrow_m H$ maps m adjacent symbols in X_S into a single granule $H_i \in H$.

For example, consider the symbolic time series C in Table II. Using $G \trianglelefteq_3 H$, a sequence mapping $g: C \rightarrow_3 H$ creates granularity H where the granules are: $H_1: \langle C:1, C:1, C:0 \rangle$, $H_2: \langle C:1, C:0, C:0 \rangle$, $H_3: \langle C:1, C:1, C:0 \rangle$, and so on.

Definition 3.10 (Temporal sequence of a symbolic time series) Consider a symbolic time series X_S of granularity G . Let $\langle \omega_1, \dots, \omega_m \rangle$ be a symbolic sequence at granule H_i in H , obtained by performing a sequence mapping $g: X_S \rightarrow_m H$. A temporal sequence $Seq_i = \langle e_1, \dots, e_n \rangle$ is a list of n event instances, each is obtained by grouping consecutive and identical symbols ω in H_i into an event instance $e = (\omega, [t_s, t_e])$.

In the previous example, the temporal sequences of the granules in H are: $Seq_1 = \langle (C:1, [G_1, G_2]), (C:0, [G_3, G_3]) \rangle$ at H_1 , $Seq_2 = \langle (C:1, [G_4, G_4]), (C:0, [G_5, G_6]) \rangle$ at H_2 , $Seq_3 = \langle (C:1, [G_7, G_8]), (C:0, [G_9, G_9]) \rangle$ at H_3 , and so on.

Definition 3.11 (Temporal sequence database) Consider a symbolic database \mathcal{D}_{SYB} of granularity G (defined in Def 3.6) which contains a collection of symbolic time series $\{X_S\}$, and a granularity $H \in \mathcal{H}$. Let $g: X_S \rightarrow_m H$ be a sequence mapping applied to each symbolic time series X_S in \mathcal{D}_{SYB} . The temporal sequences obtained from the mapping g form a temporal sequence database \mathcal{D}_{SEQ} where each row i is a set of sequences $\{Seq_i\}$ of the same granule $H_i \in H$. Furthermore, the temporal sequence database \mathcal{D}_{SEQ} has granularity H .

Table IV shows an example of \mathcal{D}_{SEQ} , obtained from \mathcal{D}_{SYB} in Table II using the mapping $g: X_S \rightarrow_3 H$ on the five symbolic time series $\{C, D, F, M, N\}$.

Given a symbolic database \mathcal{D}_{SYB} of granularity G and a granularity hierarchy \mathcal{H} , we can construct different temporal sequence databases \mathcal{D}_{SEQ} of different granularities $H \in \mathcal{H}$ by using different sequence mappings $g: X_S \rightarrow_m H$. For instance, in the previous example, using $g: X_S \rightarrow_3 H$, we obtain \mathcal{D}_{SEQ} at 15-Minutes granularity. Using $g: X_S \rightarrow_{12} H$, we obtain \mathcal{D}_{SEQ} at 1-Hour granularity.

E. Frequent Seasonal Temporal Pattern

Definition 3.12 (Support set of a temporal event) Consider a temporal sequence database \mathcal{D}_{SEQ} of granularity H , and a temporal event E . The set of granules H_i in \mathcal{D}_{SEQ} where E occurs, arranged in an increasing order, is called the support set of event E and is denoted as $\text{SUP}^E = \{H_l^E, \dots, H_r^E\}$, where $1 \leq l \leq r \leq |\mathcal{D}_{\text{SEQ}}|$. The granule H_i at which event E occurs is denoted as H_l^E . The support set of a group of events, denoted as $\text{SUP}^{\langle E_1, \dots, E_k \rangle}$, and the support set of a temporal pattern, denoted as $\text{SUP}^P = \{H_l^P, \dots, H_r^P\}$, are defined similarly to that of a temporal event.

Definition 3.13 (Near support set of a temporal pattern) Consider a pattern P with the support set $\text{SUP}^P = \{H_l^P, \dots, H_r^P\}$. Let $maxPeriod$ be the maximum period threshold, representing the predefined maximal period between any two consecutive granules in SUP^P . The set SUP^P is called a near support set of P if $\forall (H_o^P, H_p^P) \in \text{SUP}^P$: $(H_o^P$ and H_p^P are consecutive) $\wedge |p(H_o^P) - p(H_p^P)| \leq maxPeriod$, where $p(H_o^P)$ and $p(H_p^P)$ are the positions of H_o^P and H_p^P in granularity H . We denote the near support set of pattern P as NearSUP^P .

Intuitively, the near support set of P is a support set where P 's occurrences are close in time. Moreover, NearSUP^P is called a maximal near support set if NearSUP^P has no other superset beside itself which is also a near support set. The

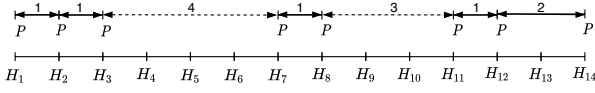


Fig. 3: Near support sets of pattern $P = (C:1 \geq D:1)$

near support set of an event is defined similarly to that of a pattern.

As an example, consider the pattern $P = (\text{Contains}, C:1, D:1)$ (or $C:1 \geq D:1$) in Table IV, and let $\text{maxPeriod} = 2$. Here, the support set of P is $\text{SUP}^P = \{H_1, H_2, H_3, H_7, H_8, H_{11}, H_{12}, H_{14}\}$. Hence, P has three maximal near support sets: $\text{NearSUP}_1^P = \{H_1, H_2, H_3\}$, $\text{NearSUP}_2^P = \{H_7, H_8\}$, and $\text{NearSUP}_3^P = \{H_{11}, H_{12}, H_{14}\}$. Fig. 3 illustrates the three near support sets of P .

Definition 3.14 (Season of a temporal pattern) Let NearSUP^P be a near support set of a pattern P . Then NearSUP^P is called a *season* of P if $\text{den}(\text{NearSUP}^P) = |\text{NearSUP}^P| \geq \text{minDensity}$, where $\text{den}(\text{NearSUP}^P)$ counts the number of granules in NearSUP^P called the *density* of NearSUP^P , and minDensity is a predefined minimum density threshold.

For instance, in the previous example, we have $\text{den}(\text{NearSUP}_1^P) = |\text{NearSUP}_1^P| = 3$. Similarly, $\text{den}(\text{NearSUP}_2^P) = 2$, $\text{den}(\text{NearSUP}_3^P) = 3$. If the occurrences of a pattern P are dense enough, the near support set becomes a season of P . Intuitively, a *season* of a temporal pattern is a *concentrated occurrence period*, separated by a long *gap period* of no/few occurrences, before the next season starts. The season of an event is defined similarly as for a pattern.

The *distance* between two seasons $\text{NearSUP}_i^P = \{H_k^P, \dots, H_n^P\}$ and $\text{NearSUP}_j^P = \{H_r^P, \dots, H_u^P\}$ is computed as: $\text{dist}(\text{NearSUP}_i^P, \text{NearSUP}_j^P) = |p(H_n^P) - p(H_r^P)|$.

Based on the season concept and the distance measure, we define frequent seasonal temporal patterns as follows.

Definition 3.15 (Frequent seasonal temporal pattern) Let $\mathcal{PS} = \{\text{NearSUP}^P\}$ be the set of seasons of a temporal pattern P , and minSeason be the *minimum seasonal occurrence* threshold, $\text{distInterval} = [\text{dist}_{\min}, \text{dist}_{\max}]$ be the *distance interval* where dist_{\min} is the minimum distance and dist_{\max} is the maximum distance. A temporal pattern P is called a *frequent seasonal temporal pattern* iff $\text{seasons}(P) = |\mathcal{PS}| \geq \text{minSeason} \wedge \forall (\text{NearSUP}_i^P, \text{NearSUP}_j^P) \in \mathcal{PS}$: they are consecutive and $\text{dist}_{\min} \leq \text{dist}(\text{NearSUP}_i^P, \text{NearSUP}_j^P) \leq \text{dist}_{\max}$.

Intuitively, a pattern P is *seasonal* if the distance between two consecutive seasons is within the predefined distance interval. Moreover, a seasonal temporal pattern is *frequent* if it occurs more often than a predefined *minimum seasonal occurrence* threshold. The number of seasons of a pattern P is the size of \mathcal{PS} , and is computed as $\text{seasons}(P) = |\mathcal{PS}|$.

Mining Frequent Seasonal Temporal Patterns from Time Series (FreqSTPfts). Given a set of n time series $\mathcal{X} = \{X_1, \dots, X_n\}$ of granularity G , let \mathcal{D}_{SEQ} be the temporal sequence database of granularity $H \in \mathcal{H}$ obtained from \mathcal{X} , and maxPeriod , minDensity , distInterval , and minSeason be the maximum period, minimum density, distance interval, and minimum seasonal occurrence thresholds, respectively.

The FreqSTPfts problem aims to find all frequent seasonal temporal patterns P in \mathcal{D}_{SEQ} that satisfy the *maxPeriod*, *minDensity*, *distInterval*, and *minSeason* constraints.

In Section VI-A, we provide the guidelines on how to set the values of the four constraints in real-life settings.

IV. FREQUENT SEASONAL TEMPORAL PATTERN MINING

A. Overview of FreqSTPfts Mining Process

The FreqSTPfts mining process consists of two phases. **Phase 1**, *Data Transformation*, converts a set of time series \mathcal{X} into a symbolic database \mathcal{D}_{SYB} by using the mapping function defined in Def. 3.5, and then converts \mathcal{D}_{SYB} into a temporal sequence database \mathcal{D}_{SEQ} by applying the sequence mapping defined in Def. 3.9. **Phase 2**, *Seasonal Temporal Pattern Mining (STPM)*, consists of two steps to mine frequent seasonal temporal patterns: *Seasonal Single Event Mining* and *Seasonal k-Event Pattern Mining* ($k \geq 2$).

Before introducing the STPM algorithm in detail, we first present *candidate seasonal pattern*, a concept designed to support Apriori-like pruning in STPM.

B. Candidate Seasonal Pattern

Pattern mining methods often use the *anti-monotonicity* property of the *support* measure to reduce the search space [44]. This property ensures that an infrequent event E_i cannot form a frequent 2-event pattern P , since $\text{support}(E_i) \geq \text{support}(P)$. Hence, if E_i is infrequent, we can safely remove E_i and any of its combinations from the search space, and still guarantee the algorithm completeness. However, seasonal temporal patterns constrained by the *maxPeriod*, *minDensity*, *distInterval* and *minSeason* thresholds do *not* uphold this property, as illustrated below.

Consider an event $E = M:1$ and a 2-event pattern $P = M:1 \geq N:1$ in Table IV. Let $\text{maxPeriod} = 2$, $\text{minDensity} = 3$, $\text{distInterval} = [4, 10]$, and $\text{minSeason} = 2$. From the constraints, we can identify the seasons of E and P as: $\mathcal{PS}^E = \{\text{NearSUP}_1^E\} = \{H_1, H_2, H_3, H_4, H_5, H_6, H_8, H_9, H_{10}, H_{11}, H_{13}\}$, and $\mathcal{PS}^P = \{\{\text{NearSUP}_1^P\} = \{H_1, H_3, H_4, H_5, H_6\}, \{\text{NearSUP}_2^P\} = \{H_{10}, H_{11}, H_{13}\}\}$. Here, for the pattern P , H_2 is not present in $\{\text{NearSUP}_1^P\}$ since P does not occur in H_2 , and H_9 is not present in $\{\text{NearSUP}_2^P\}$ because of the constraint $\text{dist}_{\min} = 4$. Hence, we have: $|\mathcal{PS}^E| = 1$ and $|\mathcal{PS}^P| = 2$. Due to the *minSeason* constraint, E is not a frequent seasonal event, whereas P is. This shows that seasonal temporal patterns do not adhere to the anti-monotonic property.

To improve STPM performance, we propose the novel *maximum seasonal occurrence* measure, called *maxSeason*, that upholds the anti-monotonicity property to prune infrequent patterns and reduce STPM search space. Indeed, *maxSeason* is an upper bound on the number of seasons of a pattern.

Maximum seasonal occurrence of a temporal pattern P : is the ratio between the number of granules in the support set SUP^P of P , and the *minDensity* threshold:

$$\text{maxSeason}(P) = \frac{|\text{SUP}^P|}{\text{minDensity}} \quad (1)$$

Eq. (1) divides the number of granules containing P by the minimum density of a season. Thus, it computes the

maximum seasons a pattern P can have. The maximum seasonal occurrence of a single event E , and of a group of events (E_i, \dots, E_k) , are defined in a similar way. Below, we show how $maxSeason$ upholds the anti-monotonicity property.

Lemma 1. *Let P and P' be two temporal patterns such that $P' \subseteq P$. Then $maxSeason(P') \geq maxSeason(P)$.*

Proof. We have:

$$maxSeason(P') = \frac{|SUP^{P'}|}{minDensity}, maxSeason(P) = \frac{|SUP^P|}{minDensity}$$

Since: $|SUP^{P'}| \geq |SUP^P|$ (Derived from Def. 3.12)

Hence: $maxSeason(P') \geq maxSeason(P)$ \square

Lemma 2. *Let P be a k -event temporal pattern formed by a k -event group (E_1, \dots, E_k) . Then, $maxSeason(P) \leq maxSeason(E_1, \dots, E_k)$.*

Proof. Derived directly from Def. 3.12, and Eq. (1). \square

From Lemmas 1 and 2, the $maxSeason$ of a pattern P is always at most the $maxSeason$ of its sub-pattern P' , and of its events (E_1, \dots, E_k) . Thus, $maxSeason$ upholds the anti-monotonicity property, and can be used to reduce the STPM search space. Below, we define the *candidate pattern* concept that uses $maxSeason$ as a gatekeeper to identify frequent/infrequent seasonal patterns.

Candidate seasonal pattern: A temporal pattern P is a *candidate seasonal pattern* if $maxSeason(P) \geq minSeason$.

Similarly, a group of k events $G_E = (E_1, \dots, E_k)$ ($k \geq 1$) is a *candidate seasonal k -event group* if $maxSeason(G_E) \geq minSeason$. Intuitively, a pattern P (or k -event group G_E) is infrequent if its $maxSeason$ is less than $minSeason$. Hence, P (or G_E) can be safely removed from the search space.

Next, we present our STPM algorithm and detail the two mining steps. Algorithm 1 provides the pseudo-code of STPM.

C. Mining Seasonal Single Events

The first step in STPM is to mine frequent seasonal single events (Alg. 1, lines 1-9) that satisfy the constraints of $maxPeriod$, $minDensity$, $distInterval$ and $minSeason$. To do that, we first look for the candidate single events defined in Section IV-B, and then use only the found candidates to mine frequent seasonal events.

The candidate single events are found by first scanning \mathcal{D}_{SEQ} to identify the support set SUP^{E_i} for each event E_i , from which we compute the maximum seasonal occurrence $maxSeason(E_i)$. If $maxSeason(E_i) \geq minSeason$, then E_i is a candidate seasonal single event. Otherwise, E_i is not a candidate and is removed from the search space. Note that we only need to scan \mathcal{D}_{SEQ} once to find all candidate events.

To mine frequent seasonal events, for each candidate event E_i , we iterate through the support set SUP^{E_i} , and calculate the period pr_{ij} between every two consecutive granules in SUP^{E_i} , and determine the near support sets $NearSUP^{E_i}$ that satisfy $maxPeriod$ and $minDensity$. Next, the set of seasons \mathcal{PS}^{E_i} is identified by selecting the near support sets that adhere to the $distInterval$ constraint. Finally, the frequent seasonal events are determined by comparing the number of

Algorithm 1: Frequent Seasonal Temporal Pattern Mining

Input: Temporal sequence database \mathcal{D}_{SEQ} , the thresholds: $maxPeriod$, $minDensity$, $distInterval$, $minSeason$

Output: The set of frequent seasonal temporal patterns \mathcal{P}
 // Step 2.1: Mining frequent seasonal single events

```

1: foreach event  $E_i \in \mathcal{D}_{SEQ}$  do
2:   Find  $SUP^{E_i}$  and compute  $maxSeason(E_i)$ ;
3:   if  $maxSeason(E_i) \geq minSeason$  then
4:     | Insert  $E_i$  into Candidate1Event;
5: foreach candidate  $E_i \in$  Candidate1Event do
6:   Find  $NearSUP^{E_i}$  that satisfies  $maxPeriod$  and  $minDensity$ ;
7:   Find  $\mathcal{PS}^{E_i}$  that adheres  $distInterval$ ;
8:   if  $|\mathcal{PS}^{E_i}| \geq minSeason$  then
9:     | Insert  $E_i$  into  $\mathcal{P}$ ; //  $E_i$  is a frequent seasonal event
10: // Step 2.2: Mining frequent seasonal  $k$ -event patterns,  $k \geq 2$ 
11: FilteredF1  $\leftarrow$  Transitivity_Filtering( $F_1$ );
12: kEventGroups  $\leftarrow$  Cartesian(FilteredF1,  $F_{k-1}$ );
13: CandidatekEvent  $\leftarrow$  maxSeason_Filtering(kEventGroups);
14: foreach kEvent in CandidatekEvent do
15:   | (k-1)-event_patterns  $\leftarrow$  Retrieve_Relations( $PH_{k-1}$ );
16:   | k-event_patterns  $\leftarrow$  Iterative_Check((k-1)-event_patterns,  $E_k$ );
17:   foreach  $P$  in k-event_patterns do
18:     | if  $maxSeason(P) \geq minSeason$  then
19:       | | Insert  $P$  into CandidatekPatterns;
20: foreach candidate  $P \in$  CandidatekPatterns do
21:   Find  $NearSUP^P$  satisfying  $maxPeriod$  and  $minDensity$ ;
22:   Identify  $\mathcal{PS}^P$  adhering to  $distInterval$ ;
23:   if  $|\mathcal{PS}^P| \geq minSeason$  then
     | Insert  $P$  into  $\mathcal{P}$ ; //  $P$  is a frequent seasonal pattern

```

seasons of E_i to $minSeason$, selecting only those that have $seasons(E_i) = |\mathcal{PS}^{E_i}| \geq minSeason$.

We use a *hierarchical lookup hash structure* $HLLH_1$ to store the candidate seasonal single events. This data structure enables fast search when mining seasonal k -events patterns ($k \geq 2$). Note that we maintain the candidate events in $HLLH_1$ instead of the frequent seasonal events, as the $maxSeason$ of candidate events upholds the anti-monotonicity property, and can thus be used for pruning. We illustrate $HLLH_1$ in Fig. 4, and describe the data structure below.

Hierarchical lookup hash structure $HLLH_1$: The $HLLH_1$ is a hierarchical data structure that consists of two hash tables: the *single event hash table* EH , and the *event granule hash table* GH . Each hash table has a list of $\langle key, value \rangle$ pairs. In EH , the key is the event symbol $\omega \in \Sigma_X$ representing the candidate E_i , and the value is the list of granules $\langle H_i, \dots, H_k \rangle$ in SUP^{E_i} . In GH , the key is the list of granules shared in the value field of EH , while the value stores event instances of E_i that appear at the corresponding granule in \mathcal{D}_{SEQ} . The $HLLH_1$ structure enables fast retrieval of event granules and instances when mining candidate seasonal k -event patterns in the next step of STPM.

We provide an example of $HLLH_1$ in Fig. 6 using data in Table IV with $maxPeriod = 2$, $minDensity = 3$, $distInterval = [4, 10]$, and $minSeason = 2$. Here, out of 10 events in \mathcal{D}_{SEQ} , we have eight candidate seasonal single events stored in $HLLH_1$: C:1, C:0, D:1, D:0, F:1, F:0, M:1, and N:1. Due to space limitations, we only provide the detailed internal structure of four candidate events. Among the eight candidates, the event M:1 does not satisfy the $minSeason$ threshold since

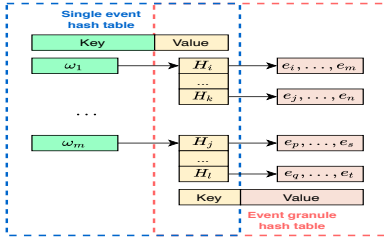


Fig. 4: The HLL_1 structure

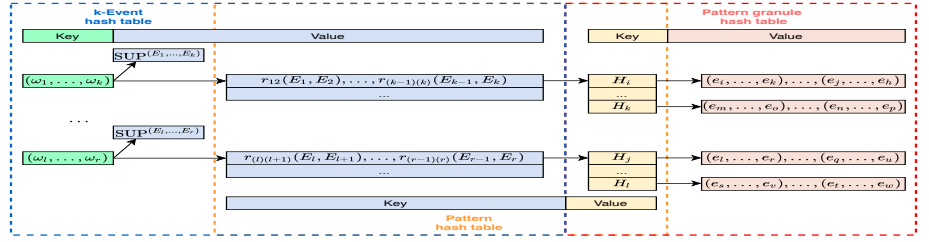


Fig. 5: The $HLL_k (k \geq 2)$ structure

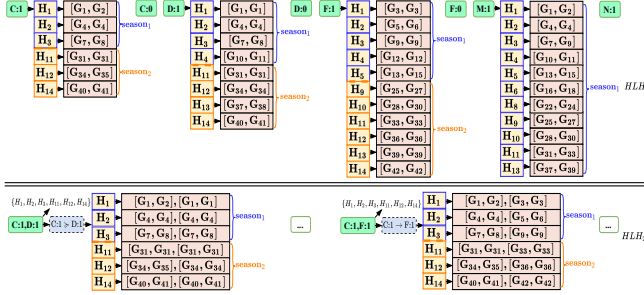


Fig. 6: A hierarchical lookup hash tables for the running example $season(M:1) = 1$, and thus, is not a frequent seasonal event. However, M:1 is still present in HLL_1 as M:1 might create frequent seasonal k-event patterns. In contrast, N:0 and M:0 are not the candidate seasonal events because they do not satisfy the $maxSeason$ constraint, and are omitted from HLL_1 .

Complexity: The complexity of finding frequent seasonal events is $O(n \cdot |\mathcal{D}_{SEQ}|)$, where n is the number of events.

Proof. (Sketch - Full proof in [43]). Computing $maxSeason$ for n events takes $O(n \cdot |\mathcal{D}_{SEQ}|)$. Identifying the set of seasons \mathcal{PS} of all candidate events E_i takes $O(n \cdot |SUP^{E_i}|)$. The overall complexity is thus: $O(n \cdot |\mathcal{D}_{SEQ}| + n \cdot |SUP^{E_i}|) \sim O(n \cdot |\mathcal{D}_{SEQ}|)$. \square

D. Mining Seasonal k-event Patterns

Search space of STPM. The next step of STPM is to mine frequent seasonal k-event patterns ($k \geq 2$). A straightforward approach is to enumerate all possible k-event combinations, and check whether each combination can form frequent seasonal patterns. However, this naive approach is very expensive as it creates a very large search space, approximately of size $O(n^h 3^{h^2})$, where n is the number of distinct events in \mathcal{D}_{SEQ} , and h is the maximal length of a temporal pattern, making it computationally prohibitive to mine seasonal patterns.

Proof. (Sketch - Full proof in [43]). The number of seasonal single events is: $N_1 = n \sim O(n)$. For mining 2-event groups, the number of 2-event groups is: $N_2 \sim O(n^2)$. Each 2-event group in N_2 can form 3 different temporal relations, and thus, the total number of seasonal 2-event patterns is: $N_2 \times 3^1 \sim O(n^2 3^1)$. Similarly, the number of seasonal h-event patterns is $O(n^h 3^{h^2})$. Therefore, the total number of seasonal temporal patterns is $O(n) + O(n^2 3^1) + \dots + O(n^h 3^{h^2}) \sim O(n^h 3^{h^2})$. \square

The problem of a large search space is thus alleviated by using an iterative mining process that first finds candidate seasonal k-event groups, and then mines frequent seasonal

k-event patterns only from the candidates. Below, we first introduce the data structure used in this mining step.

The hierarchical lookup hash structure HLL_k : We use the *hierarchical lookup hash structure* HLL_k ($k \geq 2$) to maintain candidate seasonal k-event groups and patterns, as illustrated in Fig. 5. The HLL_k contains three hash tables: the *k-event hash table* EH_k , the *pattern hash table* PH_k , and the *pattern granule hash table* GH_k . For each $\langle key, value \rangle$ pair of EH_k , *key* is the list of symbols $(\omega_1, \dots, \omega_k)$ representing the candidate k-event group (E_1, \dots, E_k) , and *value* is an *object* which consists of two components: (1) the support set $SUP^{(E_1, \dots, E_k)}$, and (2) a list of candidate seasonal k-event temporal patterns. In PH_k , *key* is the candidate pattern P which indeed takes the *value* component of EH_k , while *value* is the list of granules that contain P . In GH_k , *key* is the list of granules containing P which indeed takes the *value* component of PH_k , while *value* is the list of event instances from which the temporal relations in P are formed. The HLL_k hash structure helps speed up the candidate seasonal k-event group mining through the use of the support set in EH_k , and enables fast search for temporal relations between k events using the information in PH_k and GH_k .

4.1 Mining candidate seasonal k-event groups. We first find candidate seasonal k-event groups (Alg. 1, lines 10-12).

Let F_{k-1} be the set of candidate seasonal (k-1)-event groups found in HLL_{k-1} , and F_1 be the set of candidate seasonal single events in HLL_1 . We first generate all possible k-event groups by computing the Cartesian product $F_{k-1} \times F_1$. Next, for each k-event group (E_1, \dots, E_k) , we compute the support set $SUP^{(E_1, \dots, E_k)}$ by taking the *intersection* between $SUP^{(E_1, \dots, E_{k-1})}$ in EH_{k-1} and SUP^{E_k} in EH . We then compute $maxSeason(E_1, \dots, E_k)$, and evaluate whether (E_1, \dots, E_k) is a candidate k-event group, i.e., $maxSeason(E_1, \dots, E_k) \geq minSeason$. If (E_1, \dots, E_k) is a candidate, it is kept in EH_k of HLL_k .

4.2 Mining frequent seasonal k-event patterns. We use the found candidate k-event groups to mine frequent seasonal k-event patterns (Alg. 1, lines 13-23). We first discuss the case of 2-event patterns, and then generalize to k-event patterns.

4.2.1 Mining frequent seasonal 2-event patterns: For each candidate 2-event group (E_i, E_j) , we use the support set $SUP^{(E_i, E_j)}$ to retrieve the temporal sequences \mathcal{S} that contain (E_i, E_j) . Next, for each sequence $S \in \mathcal{S}$, we extract their event instances (e_i, e_j) , and verify the relation between them. We then compute the $maxSeason$ of the 2-event pattern P and determine if P is a candidate pattern, i.e., $maxSeason(P) \geq minSeason$. Finally, the candidate seasonal 2-event patterns are

stored in PH_2 , while their event instances are stored in GH_2 .

Based on the set of candidate seasonal 2-event patterns P , we determine whether P is a frequent seasonal 2-event pattern by checking the constraints of $maxPeriod$, $minDensity$, $distInterval$ and $minSeason$ as in the case of single events, using the support set SUP^P retrieved from the value of PH_2 .

4.2.2 Mining frequent seasonal k-event patterns: Let $N_{k-1} = (E_1, \dots, E_{k-1})$ be a candidate (k-1)-event group in HLH_{k-1} , $N_1 = (E_k)$ be a candidate single event in HLH_1 , and $N_k = N_{k-1} \cup N_1 = (E_1, \dots, E_k)$ be a candidate k-event in HLH_k . To find k-event patterns for N_k , we first retrieve the set of candidate (k-1)-event patterns \mathcal{P}_{k-1} by accessing the EH_{k-1} table. Each $P_{k-1} \in \mathcal{P}_{k-1}$ is a list of $\frac{1}{2}(k-1)(k-2)$ triples: $\{(r_{12}, E_1, E_2), \dots, (r_{(k-2)(k-1)}, E_{k-2}, E_{k-1})\}$. We iteratively verify the possibility of P_{k-1} forming a k-event pattern P_k with E_k as follows.

We first start with the triple $(r_{(k-1)k}, E_{k-1}, E_k)$. If $(r_{(k-1)k}, E_{k-1}, E_k)$ does not exist in HLH_2 , then P_k is not a candidate k-event pattern, and the verification stops immediately. Otherwise, we continue the similar verification on the triple $(r_{(k-2)k}, E_{k-2}, E_k)$, until it reaches (r_{1k}, E_1, E_k) . Next, we compute $maxSeason(P_k)$ to determine whether P_k is a candidate k-event pattern, i.e., $maxSeason(P_k) \geq minSeason$. The candidate k-event patterns are maintained in PH_k and GH_k . Finally, we mine frequent seasonal k-event patterns from the found candidates, similar to 2-event patterns.

Using transitivity property to optimize candidate k-event groups: In Section 4.1, when mining candidate k-event groups, we perform the Cartesian product between F_{k-1} and F_1 . However, using the candidate single events in F_1 to generate k-event groups can create redundancy, since events in F_1 when combined with F_{k-1} might not form any frequent seasonal k-event patterns. For example, consider the event F:0 in HLH_1 in Fig. 6. Here, F:0 is a candidate single event, and thus, can be combined with 2-event groups in HLH_2 such as (C:1, D:1) to create a 3-event group (C:1, D:1, F:0). However, (C:1, D:1, F:0) cannot form any candidate seasonal 3-event patterns, since F:0 is not present in any candidate 2-event patterns in HLH_2 . To reduce such redundancy and further optimize the mining, we use the *transitivity property* of temporal relations to identify such event groups.

Lemma 3. Let $S = \langle e_1, \dots, e_{k-1} \rangle$ be a temporal sequence, $P = \langle (r_{12}, E_{1 \triangleright e_1}, E_{2 \triangleright e_2}), \dots, (r_{(k-2)(k-1)}, E_{k-2 \triangleright e_{k-2}}, E_{k-1 \triangleright e_{k-1}}) \rangle$ be a (k-1)-event pattern that occurs in S , e_k be a new event instance added to S to create the temporal sequence $S' = \langle e_1, \dots, e_k \rangle$. The set of temporal relations \mathfrak{R} is transitive on S' : $\forall e_i \in S', i < k, \exists r \in \mathfrak{R}$ s.t. $r(E_{i \triangleright e_i}, E_{k \triangleright e_k})$ hold.

Lemma 3 states the temporal transitivity property between temporal events, and is used to prove the following lemma.

Lemma 4. Let $N_{k-1} = (E_1, \dots, E_{k-1})$ be a candidate seasonal (k-1)-event group, and E_k be a candidate seasonal single event. The group $N_k = N_{k-1} \cup E_k$ can form candidate seasonal k-event temporal patterns if $\forall E_i \in N_{k-1}, \exists r \in \mathfrak{R}$ s.t. $r(E_i, E_k)$ is a candidate seasonal temporal relation.

From Lemma 4, only single events in HLH_1 that occur in HLH_{k-1} should be used to create k-event groups. We identify these single events by filtering F_1 , and creating the set $FilteredF1$. Then, the Cartesian product $F_{k-1} \times F_1$ is replaced by $F_{k-1} \times FilteredF1$ to generate k-event groups.

Complexity: Let n be the number of single events in HLH_1 , i be the average number of instances of each event, r be the number of (k-1)-event patterns in HLH_{k-1} , and u be the average number of granules of each event/ temporal relation. The complexity of frequent seasonal k-event pattern mining is $O(n^2 i^2 u^2) + O(|F_1| \cdot |F_{k-1}| \cdot r \cdot k^2 \cdot u)$.

Proof. (Sketch - Full proof in [43]). Computing $maxSeason$ of 2-event patterns takes $O(n^2 i^2 u^2)$. Identifying the set of seasons \mathcal{PS} of candidate 2-event patterns takes $O(n^2 u)$. The complexity of frequent seasonal 2-event pattern mining is: $O(n^2 i^2 u^2 + n^2 u) \sim O(n^2 i^2 u^2)$. Computing $maxSeason$ of k-event patterns ($k > 2$) takes $O(|F_1| \cdot |F_{k-1}| \cdot r \cdot k^2 \cdot u)$. Identifying the set of seasons \mathcal{PS} of candidate k-event patterns takes $O(|F_1| \cdot |F_{k-1}| \cdot r \cdot u)$. The complexity of frequent seasonal k-event pattern mining is: $O(|F_1| \cdot |F_{k-1}| \cdot r \cdot k^2 \cdot u + |F_1| \cdot |F_{k-1}| \cdot r \cdot u) \sim O(|F_1| \cdot |F_{k-1}| \cdot r \cdot k^2 \cdot u)$. Thus, the total time complexity is $O(n^2 i^2 u^2) + O(|F_1| \cdot |F_{k-1}| \cdot r \cdot k^2 \cdot u)$. \square

STPM overall complexity: The space complexity of STPM is $O(n^h 3^{h^2})$. The time complexity of STPM depends on the size of the search space $O(n^h 3^{h^2})$, i.e., STPM scales exponentially with quadratic exponent in the pattern length h , and on the complexity of the mining process itself, i.e., $O(n \cdot |\mathcal{D}_{SEQ}|) + O(n^2 i^2 u^2) + O(|F_1| \cdot |F_{k-1}| \cdot r \cdot k^2 \cdot u)$. While the parameters n, h, i, r and k depend on the number of time series, others such as $|F_1|, |F_{k-1}|$ and u depend on the number of temporal sequences. Thus, STPM space and time complexities are driven by two main factors: the number of time series and the number of temporal sequences.

V. APPROXIMATE STPM

A. Correlated Symbolic Time Series

Let X_S and Y_S be the symbolic series representing the time series X and Y , and Σ_X, Σ_Y be their symbolic alphabets.

Definition 5.1 (Entropy) The *entropy* of X_S , denoted as $H(X_S)$, is defined as

$$H(X_S) = - \sum_{x \in \Sigma_X} p(x) \cdot \log p(x) \quad (2)$$

where $p(x)$ is the probability of X_S . Intuitively, the entropy measures the uncertainty of the possible outcomes of X_S [45].

The *conditional entropy* $H(X_S|Y_S)$ is defined as

$$H(X_S|Y_S) = - \sum_{x \in \Sigma_X} \sum_{y \in \Sigma_Y} p(x, y) \cdot \log \frac{p(x, y)}{p(y)} \quad (3)$$

where $p(x, y)$ is the joint probability of (X_S, Y_S) , and $p(y)$ is the probability of Y_S .

Definition 5.2 (Mutual information) The *mutual information* (MI) of two symbolic series X_S and Y_S , denoted as $I(X_S; Y_S)$, is defined as

$$I(X_S; Y_S) = \sum_{x \in \Sigma_X} \sum_{y \in \Sigma_Y} p(x, y) \cdot \log \frac{p(x, y)}{p(x) \cdot p(y)} \quad (4)$$

The MI represents the reduction of uncertainty of one variable (e.g., X_S), given the knowledge of another variable (e.g., Y_S).

The larger $I(X_S; Y_S)$, the more information is shared between X_S and Y_S . Since $0 \leq I(X_S; Y_S) \leq \min\{H(X_S), H(Y_S)\}$ [45], the MI value has no upper bound. To scale it into the range $[0 - 1]$, we normalize the MI as defined below.

Definition 5.3 (Normalized mutual information) The *normalized mutual information* (NMI) of two symbolic time series X_S and Y_S , denoted as $\tilde{I}(X_S; Y_S)$, is defined as

$$\tilde{I}(X_S; Y_S) = \frac{I(X_S; Y_S)}{H(X_S)} = 1 - \frac{H(X_S|Y_S)}{H(X_S)} \quad (5)$$

$\tilde{I}(X_S; Y_S)$ represents the reduction (in percentage) of the uncertainty of X_S due to knowing Y_S . Based on Eq. (5), a pair of variables (X_S, Y_S) has a mutual dependency if $\tilde{I}(X_S; Y_S) > 0$. Moreover, Eq. (5) also shows that NMI is not symmetric, i.e., $\tilde{I}(X_S; Y_S) \neq \tilde{I}(Y_S; X_S)$.

Definition 5.4 (Correlated symbolic time series) Let μ ($0 < \mu \leq 1$) be the mutual information threshold. We say that X_S and Y_S are *correlated* iff $\min\{\tilde{I}(X_S; Y_S), \tilde{I}(Y_S; X_S)\} \geq \mu$, and *uncorrelated* otherwise.

B. Lower Bound of the maxSeason

Consider two symbolic series X_S and Y_S . Let X_1 be a temporal event in X_S , Y_1 be a temporal event in Y_S , \mathcal{D}_{SYB} and \mathcal{D}_{SEQ} be the symbolic and the sequence databases created from X_S and Y_S , respectively. We have the following relation between $\tilde{I}(X_S; Y_S)$ in \mathcal{D}_{SYB} , and $\maxSeason(X_1, Y_1)$ in \mathcal{D}_{SEQ} .

Theorem 1. (Lower bound of the maximum seasonal occurrence) Let μ be the mutual information threshold. If the NMI $\tilde{I}(X_S; Y_S) \geq \mu$, then the maximum seasonal occurrence of (X_1, Y_1) in \mathcal{D}_{SEQ} has a lower bound:

$$\maxSeason(X_1, Y_1) \geq \frac{\lambda_2 \cdot |\mathcal{D}_{SEQ}|}{\minDensity} \cdot e^{W\left(\frac{\log \lambda_1^{1-\mu} \cdot \ln 2}{\lambda_2}\right)} \quad (6)$$

where: $\lambda_1 = \min\{p(X_i), \forall X_i \in X_S\}$ is the minimum probability of $X_i \in X_S$, and $\lambda_2 = p(Y_1)$ is the probability of $Y_1 \in Y_S$, and W is the Lambert function [46].

Proof. (Sketch - Full proof in [43]). From Eq. (5), we have:

$$\begin{aligned} \tilde{I}(X_S; Y_S) &= 1 - \frac{H(X_S|Y_S)}{H(X_S)} \geq \mu \quad (7) \\ \Rightarrow \frac{H(X_S|Y_S)}{H(X_S)} &= \frac{p(X_1, Y_1) \cdot \log p(X_1|Y_1)}{\sum_i p(X_i) \cdot \log p(X_i)} \\ &+ \frac{\sum_{i \neq 1 \& j \neq 1} p(X_i, Y_j) \cdot \log \frac{p(X_i, Y_j)}{p(Y_j)}}{\sum_i p(X_i) \cdot \log p(X_i)} \leq 1 - \mu \quad (8) \end{aligned}$$

Let: $\lambda_1 = \min\{p(X_i), \forall i\}$, $\lambda_2 = p(Y_1)$.

$$\frac{H(X_S|Y_S)}{H(X_S)} \geq \frac{p(X_1, Y_1) \cdot \log \frac{p(X_1, Y_1)}{\lambda_2}}{\log \lambda_1} \quad (9)$$

From Eqs. (8), (9), we derive: $p(X_1, Y_1) \geq \lambda_2 \cdot e^{W\left(\frac{\log \lambda_1^{1-\mu} \cdot \ln 2}{\lambda_2}\right)}$

Since: $\frac{|SUP(X_1, Y_1)|}{|\mathcal{D}_{SEQ}|} \geq p(X_1, Y_1) \geq \lambda_2 \cdot e^{W\left(\frac{\log \lambda_1^{1-\mu} \cdot \ln 2}{\lambda_2}\right)}$

Thus: $\maxSeason(X_1, Y_1) \geq \frac{\lambda_2 \cdot |\mathcal{D}_{SEQ}|}{\minDensity} \cdot e^{W\left(\frac{\log \lambda_1^{1-\mu} \cdot \ln 2}{\lambda_2}\right)} \quad (10)$

□

Setting the parameters: To compute the lower bound of $\maxSeason(X_1, Y_1)$ in Eq. (6), several parameters need to be

Algorithm 2: Approximate STPM using MI

Input: A set of time series \mathcal{X} , the thresholds: \maxPeriod , \minDensity , distInterval , \minSeason

Output: The set of frequent seasonal temporal patterns \mathcal{P}
// Find the correlated symbolic series

```

1: foreach pair of symbolic time series  $(X_S, Y_S) \in \mathcal{D}_{SYB}$  do
2:    $\minNMI \leftarrow \min\{\tilde{I}(X_S; Y_S), \tilde{I}(Y_S; X_S)\}$ ;
3:   Compute  $\mu$  using Eq. (11);
4:   if  $\minNMI \geq \mu$  then
5:     | Insert  $X_S$  and  $Y_S$  into  $\mathcal{X}_C$ ;
6: Mine frequent seasonal single events from  $\mathcal{X}_C$ ;
7: foreach  $(X_S, Y_S) \in \mathcal{X}_C$  do
8:   | Mine frequent seasonal 2-event patterns from  $(X_S, Y_S)$ ;
9:   if  $k \geq 3$  then
10:  | Perform STPM using  $HLH_1$  and  $HLH_{k-1}$ ;

```

defined: λ_1 , λ_2 , and μ . Given \mathcal{D}_{SYB} , λ_1 and λ_2 can easily be determined since λ_1 is the minimum probability among all events $X_i \in X_S$, and λ_2 is the probability of $Y_1 \in Y_S$. To set the value of μ , we use the lower bound of \maxSeason in Theorem 1 to derive μ as follows.

Corollary 1.1. The maximum seasonal occurrence of an event pair $(X_1, Y_1) \in (X_S, Y_S)$ in \mathcal{D}_{SEQ} is at least \minSeason if $\tilde{I}(X_S; Y_S)$ is at least μ , where:

$$\mu \geq \begin{cases} 1 - \frac{\lambda_2}{e \cdot \ln 2 \cdot \log \frac{1}{\lambda_1}}, & \text{if } 0 \leq \rho \leq \frac{1}{e} \\ 1 - \frac{\rho \cdot \lambda_2 \cdot \log \frac{\rho}{\lambda_1}}{\ln 2 \cdot \log \frac{\rho}{\lambda_1}}, & \text{otherwise} \end{cases}, \text{ where } \rho = \frac{\minSeason \cdot \minDensity}{\lambda_2 \cdot |\mathcal{D}_{SEQ}|} \quad (11)$$

Note that μ in Eq. (11) only ensures that the \maxSeason of the pair (X_1, Y_1) is at least \minSeason . Thus, given (X_S, Y_S) , μ has to be computed for each event pair in (X_S, Y_S) . The final chosen μ value to be compared against $\tilde{I}(X_S; Y_S)$ is the minimum μ value among all the event pairs in (X_S, Y_S) .

Interpretation of the lower bound of the maximum seasonal occurrence: Theorem 1 says that, given an MI threshold μ , if the two symbolic series X_S and Y_S are correlated, i.e., $\tilde{I}(X_S; Y_S) \geq \mu$, then the maximum seasonal occurrence of an event pair in (X_S, Y_S) is at least the lower bound in Eq. (6). Combining Theorem 1 and Lemma 2, we can conclude that given a pair of symbolic series (X_S, Y_S) , if its event pair (X_1, Y_1) has a maximum seasonal occurrence less than the lower bound in Eq. (6), then any 2-event pattern P formed by that event pair also has a maximum seasonal occurrence less than that lower bound. This allows us to construct the approximate STPM algorithm, discussed in the next section.

C. Using the Bound to Approximate STPM

Approximate STPM: We construct an approximate version of STPM using Theorem 1. Specifically, using the STPM thresholds \minSeason and \minDensity , we derive μ (Eq. 11) and use it to identify *correlated symbolic series* (defined in Def. 5.4). Next, the approximate STPM performs the mining only on the set of correlated symbolic series $\mathcal{X}_C \subseteq \mathcal{X}$. Algorithm 2 outlines the approximate STPM.

First, NMI and μ are computed for each pair of symbolic series (X_S, Y_S) in \mathcal{D}_{SYB} (lines 2-3). Then, only pairs whose $\min\{\tilde{I}(X_S; Y_S), \tilde{I}(Y_S; X_S)\}$ is at least μ are inserted into \mathcal{X}_C . Next, only the correlated symbolic series in \mathcal{X}_C are used to mine frequent seasonal single events (line 6). For frequent seasonal 2-event patterns, we mine frequent seasonal patterns

only from event pairs in \mathcal{X}_C (lines 7-8). For frequent seasonal k -event patterns ($k \geq 3$), the exact STPM is used (lines 9-10).

Complexity analysis of approximate STPM: The approximate STPM differs from STPM in two mining steps, the seasonal single events at HLH_1 and the seasonal 2-event patterns at HLH_2 by mining those only from correlated time series. To compute NMI and μ , the approximate STPM only need to scan \mathcal{D}_{SYB} once to calculate the probability for each single event and event pairs. Thus, the cost of NMI and μ computations is $O(|\mathcal{D}_{SYB}|)$. In contrast, the complexities of the exact STPM at HLH_1 and HLH_2 are $O(n \cdot |\mathcal{D}_{SEQ}|) + O(n^2 i^2 u^2)$ (Sections IV-C and IV-D). Thus, the more time series are pruned, the faster and less memory usage of the approximate STPM. However, overall, the approximate STPM still scales exponentially with quadratic exponent in the pattern length h as in STPM.

VI. EXPERIMENTAL EVALUATION

Due to space limitations, we only present here the most important results, and discuss other findings in [43].

A. Experimental Setup

Datasets: We use three real-world datasets from three application domains: renewable energy, smart city, and health. For *renewable energy* (RE), we use energy data [47] and weather data [6] from Spain. For *smart city* (SC), we use traffic and weather datasets [48] from New York City. For *health*, we combine the *influenza* (INF) and *hand-foot-mouth* (HFM) datasets [5] and weather data [6] from Kawasaki, Japan. Besides real-world datasets, we also generate synthetic data for the scalability evaluation. Specifically, starting from each real-world dataset, we generate 1,000 *times more sequences* and 10,000 *synthetic time series* for each of them. Table V summarizes the dataset characteristics.

Baseline method: Our exact method is referred to as E-STPM, and the approximate one as A-STPM. Since our work is the first that studies frequent seasonal temporal pattern mining, there does not exist an exact baseline to compare against STPM. However, we adapt the state-of-the-art method for recurring itemset mining PS-growth [40] to find seasonal temporal patterns. Specifically, the adaptation is done through 2-phase process: (1) PS-growth is applied to find frequent recurring events, and (2), mine temporal patterns from extracted events. The adapted PS-growth is referred to as APS-growth.

Infrastructure: We use a virtual machine with 32 AMD EPYC cores (2GHz), 512 GB RAM, and 1 TB storage.

Parameters: Table VI lists the parameters and their values used in our experiments, where *maxPeriod* and *minDensity* are expressed as the percentage of \mathcal{D}_{SEQ} . While the four parameters in Table VI are user-defined, we also provide the intuition of how to set them. *maxPeriod* determines how close the patterns should occur within the same season. The smaller the *maxPeriod*, the closer the occurred patterns should be and vice versa. *minDensity* decides how dense a season should be. Combining these two, a small *maxPeriod* and a large *minDensity* will find dense seasons with close-by pattern occurrences. In contrast, a large *maxPeriod* and a small *minDensity* will find

TABLE V: Characteristics of the Datasets

Datasets	#seq.	#time series	#events	#ins./seq.
RE (real)	1,460	21	102	93
SC (real)	1,249	14	56	55
INF (real)	608	25	124	48
HFM (real)	730	24	115	40
RE (syn.)	$1,460 \times 10^3$	10^4	48,500	38,012
SC (syn.)	$1,249 \times 10^3$	10^4	40,020	37,106
INF (syn.)	608×10^3	10^4	49,600	40,623
HFM (syn.)	730×10^3	10^4	47,825	41,241

sparse seasons. On the other hand, *minSeason* and *distInterval* values often depend on the granularity of \mathcal{D}_{SEQ} . For example, if \mathcal{D}_{SEQ} has month granularity, we then can look for patterns with yearly seasonality. Thus, *distInterval* is often between 3 and 9 months, and *minSeason* is the minimum number of years the patterns should have occurred seasonally.

B. Qualitative Evaluation

Table VIII lists some seasonal patterns found in the datasets. Patterns P1-P3 are extracted from RE, showing that high renewable energy generation and high electricity demand occur seasonally and often at specific *season* throughout the year. Patterns P4-P7 are extracted from INF and HFM, showing the detection of seasonal diseases. Finally, how weather affects traffic is shown in patterns P8-P11 extracted from SC.

Tables IX and X list the number of seasonal patterns found in the RE and INF datasets. It can be seen that high *minSeason* leads to less generated patterns, as many have few seasonal occurrences. Moreover, high *minDensity* also generates fewer patterns since only few patterns have high occurrence density. Finally, high *maxPeriod* results in more generated patterns, since high *maxPeriod* allows more temporal relations to be formed, thus increasing the number of patterns.

C. Quantitative Evaluation

1) *Baseline comparison on real-world datasets:* We compare E-STPM and A-STPM with the baseline in terms of the runtime and memory usage. Figs. 7, 8, 9 and 10 show the comparison on RE and INF datasets. The results on other datasets are reported in the technical report [43]. Note that Figs. 7-14 use the same legend.

As shown in Figs. 7 and 8, A-STPM achieves the best runtime among all methods, and E-STPM has better runtime than the baseline. On the tested datasets, the range and average speedups of A-STPM compared to other methods are: [1.5-4.7] and 2.6 (E-STPM), and [5.2-10.6] and 7.1 (APS-growth). The speedup of E-STPM compared to the baseline is [3.5-7.2] and 4.3 on average. Note that the times to compute MI and μ for RE and INF in Figs. 7 and 8 are only 2.6 and 1.4 seconds, respectively. Moreover, A-STPM is most efficient, i.e., achieves highest speedup and memory saving, when the *minSeason* threshold is low, e.g., *minSeason* = 4. This is because there are typically many patterns with few seasonal occurrences. Thus, using A-STPM to prune uncorrelated time series early helps save computational time and resources. However, the speedup comes at the cost of a small loss in accuracy (discussed in Section VI-C4).

In terms of memory consumption, as shown in Figs. 9 and 10, A-STPM is the most efficient method, while E-STPM is more efficient than the baseline. The range and the average memory consumption of A-STPM compared to other methods

TABLE VI: Parameters and values

Params	Values (User-defined)
maxPeriod	0.2%, 0.4%, 0.6%, 0.8%, 1.0%
minDensity	0.5%, 0.75%, 1.0%, 1.25%, 1.5%
minSeason	4, 8, 12, 16, 20
distInterval	[90, 270] (RE, SC), [30, 90] (INF, HFM)

TABLE VII: A-STPM Accuracy

# minSeason	minDensity (%)					
	RE (real)			INF (real)		
	0.5	0.75	1	0.5	0.75	1
8	81	82	86	81	83	87
12	84	86	92	88	90	93
16	94	95	100	95	96	100
20	97	100	100	100	100	100

TABLE VIII: Summary of Interesting Seasonal Patterns

Patterns	minDensity (%)	maxPeriod (%)	# minSeason	Seasonal occurrence
(P1) Strong Wind \succ High Wind Power Generation	0.5	0.4	12	December, January, February
(P2) Low Temperature \succ High Energy Consumption	0.5	0.4	12	December, January, February
(P3) Very Few Clouds \succ Very High Temperature $\hat{}$ High Solar Power Generation	0.75	0.6	8	July, August
(P4) High Humidity $\hat{}$ Very Low Temperature \rightarrow Very High Influenza Cases	0.5	0.4	12	January, February
(P5) Strong Wind \succ Heavy Rain \succ High Influenza Cases	0.5	0.4	12	January, February
(P6) Low Humidity \succ High Temperature \succ Very High Hand-Foot-Mouth Disease Cases	1.0	0.6	12	May, June
(P7) Very High Temperature \succ High Wind \succ High Hand-Foot-Mouth Disease Cases	1.0	0.6	12	May, June
(P8) High Temperature \succ Strong Wind \rightarrow High Congestion	0.5	0.6	8	July, August
(P9) Strong Wind \succ Unclear Visibility \succ High Congestion	0.5	0.6	8	July, August
(P10) Heavy Rain \succ Unclear Visibility \succ High Lane-Blocked	0.4	0.8	8	July, August
(P11) Heavy Rain \succ Strong Wind \succ High Flow-Incident	0.4	0.8	8	July, August

TABLE IX: The Number of Seasonal Patterns on RE

maxPeriod (%)	minSeason (#) - minDensity (%)								
	8-0.5	8-0.75	8-1.0	12-0.5	12-0.75	12-1.0	16-0.5	16-0.75	16-1.0
0.2	35626	20427	11339	21309	12941	6935	8045	4218	3018
0.4	41462	29729	14281	25207	17381	7294	10261	7480	5483
0.6	48651	35018	16247	31860	24627	9826	14061	9738	7409

TABLE X: The Number of Seasonal Patterns on INF

maxPeriod (%)	minSeason (#) - minDensity (%)								
	8-0.5	8-0.75	8-1.0	12-0.5	12-0.75	12-1.0	16-0.5	16-0.75	16-1.0
0.2	7812	5704	4285	5159	3163	2157	3521	2105	1284
0.4	10581	8294	6535	7952	5863	4068	5293	4618	2690
0.6	12084	9618	8260	11850	8591	6028	6809	5073	3529

TABLE XI: Pruned Time Series and Events from A-STPM

# Attr.	RE						INF					
	Pruned Time Series (%)			Pruned Events (%)			Pruned Time Series (%)			Pruned Events (%)		
	12-0.5%	16-0.75%	20-1.0%	12-0.5%	16-0.75%	20-1.0%	12-0.5%	16-0.75%	20-1.0%	12-0.5%	16-0.75%	20-1.0%
2000	35.20	32.10	26.80	27.22	23.53	19.03	42.60	36.75	29.70	28.63	26.12	22.10
4000	33.05	29.15	22.05	25.24	22.41	17.95	35.70	31.03	24.80	27.35	25.77	22.01
6000	30.25	26.32	19.55	24.75	21.60	17.28	33.22	28.78	22.13	26.98	25.29	20.81
8000	29.48	25.38	19.15	24.70	21.12	16.96	31.75	28.51	21.58	26.74	24.52	20.74
10000	28.39	24.87	18.91	24.50	21.07	16.69	31.06	26.48	21.15	26.61	24.36	20.27

TABLE XII: The Accuracy of A-STPM on Syn. Data

# Attr.	RE						INF					
	Accuracy (%)						Accuracy (%)					
	12-0.5%	16-0.75%	20-1.0%	12-0.5%	16-0.75%	20-1.0%	12-0.5%	16-0.75%	20-1.0%	12-0.5%	16-0.75%	20-1.0%
2000	85	96	100	89	96	100	85	96	100	89	96	100
4000	86	96	100	90	98	100	86	96	100	90	98	100
6000	86	96	100	91	98	100	86	96	100	91	98	100
8000	88	97	100	93	98	100	88	97	100	93	98	100
10000	89	98	100	93	98	100	89	98	100	93	98	100

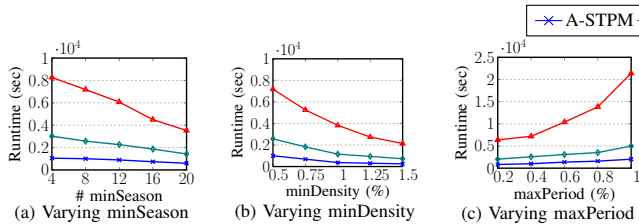


Fig. 7: Runtime Comparison on RE (real-world)

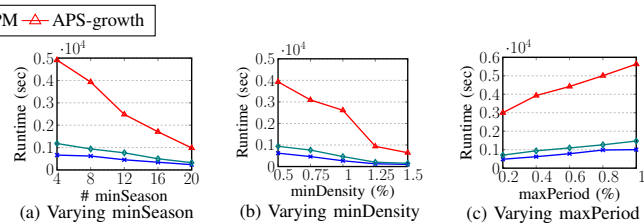


Fig. 8: Runtime Comparison on INF (real-world)

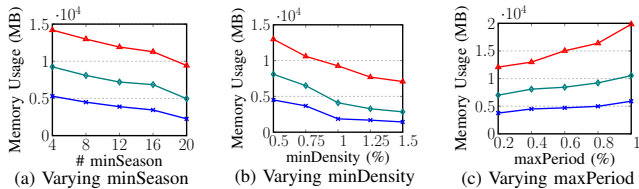


Fig. 9: Memory Usage Comparison on RE (real-world)

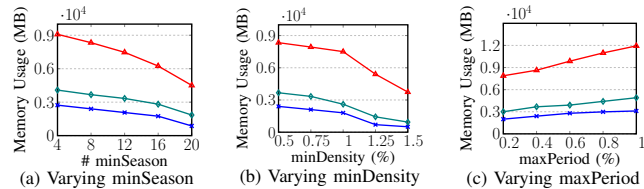


Fig. 10: Memory Usage Comparison on INF (real-world)

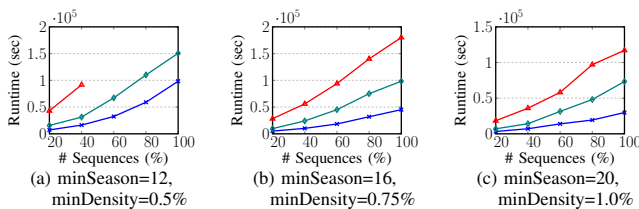


Fig. 11: Scalability: Varying #Sequences on RE (synthetic)

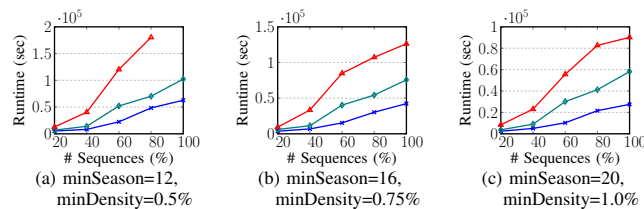


Fig. 12: Scalability: Varying #Sequences on INF (synthetic)

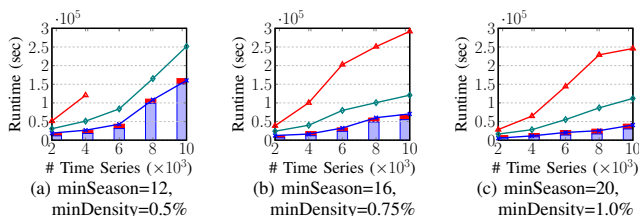


Fig. 13: Scalability: Varying #TimeSeries on RE (synthetic)

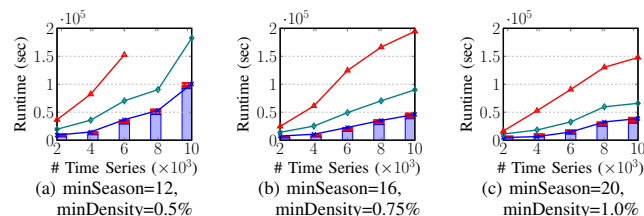


Fig. 14: Scalability: Varying #TimeSeries on INF (synthetic)

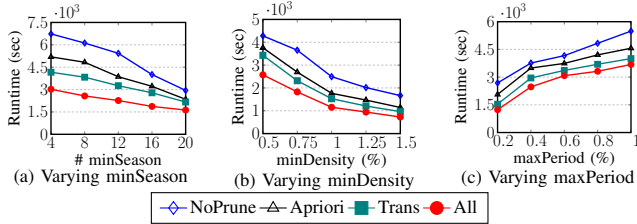


Fig. 15: Pruning Techniques of E-STPM on RE (real-world)

are: [1.4-2.7] and 1.8 (E-STPM), and [2.7-7.6] and 3.9 (APS-growth). The memory usage of E-STPM compared to the baseline is [1.5-4.1] and 2.3 on average.

2) *Scalability evaluation on synthetic datasets*: As discussed in Section IV, the complexity of STPM is driven by two main factors: (1) the number of temporal sequences, and (2) the number of time series. Thus, to further evaluate STPM scalability, we scale these two factors on synthetic datasets (reported in Table V), using two configurations: varying the number of sequences, and varying the number of time series.

Figs. 11 and 12 show the runtimes of A-STPM, E-STPM and the baseline when the number of sequences changes. We obtain the range and average speedups of A-STPM are: [1.6-3.2] and 2.2 (E-STPM), and [3.1-6.4] and 4.6 (APS-growth). Similarly, the range and average speedup of E-STPM compared to APS-growth is [1.9-4.3] and 3.2. We note that the baseline fails for larger configurations because of memory in this scalability study, i.e., on the synthetic RE at 60% sequences ($\approx 8 \times 10^5$) (Fig. 11a) and on the synthetic INF at 100% sequences ($\approx 6 \times 10^5$) (Fig. 12a), showing that A-STPM and E-STPM can scale well on big datasets while the baseline cannot.

Figs. 13 and 14 compare the runtimes of A-STPM, E-STPM and APS-growth when changing the number of time series. We obtain the range and average speedups of A-STPM are: [1.7-3.5] and 2.3 (E-STPM), and [3.8-9.5] and 5.3 (APS-growth), and of E-STPM is [2.3-4.4] and 3.6 (APS-growth). The baseline also fails at large configurations in this study, i.e., when # Time Series ≥ 6000 on the synthetic RE (Fig. 13a), and ≥ 8000 on the synthetic INF (Fig. 14a).

Furthermore, we provide the computation time of MI and μ in Figs. 13 and 14 by adding an additional bar chart for A-STPM. Each bar represents the runtime of A-STPM with two separate components: the time to compute MI and μ (top red), and the mining time (bottom blue). We note that for each dataset, we only need to compute MI once (the computed MIs are used across different $minSeason$ and $minDensity$ thresholds), while the computation of μ is negligible (in milliseconds using Eq. (11)). Thus, the MI and μ computation times, for example, in Figs. 13a, 13b, and 13c, are added only for comparison and are not all actually used.

Finally, we provide the percentage of time series and events pruned by A-STPM in the scalability test in Table XI. Here, we can see that low $minSeason$ and $minDensity$ lead to more time series (events) to be pruned. This is because $minSeason$ and $minDensity$ have an inverse relationship with μ , therefore, low $minSeason$ and $minDensity$ result in higher μ , and thus,

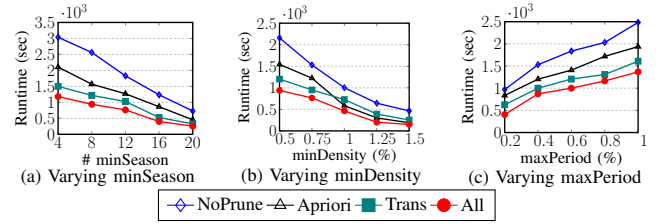


Fig. 16: Pruning Techniques of E-STPM on INF (real-world)

more pruned time series.

3) *Evaluation of the pruning techniques in E-STPM*: To understand how effective the proposed pruning techniques are, we compare different versions of E-STPM: (1) No-Prune: E-STPM with no pruning, (2) Apriori: E-STPM with Apriori-liked pruning (Lemmas 1, 2), (3) Trans: E-STPM with transitivity-based pruning (Lemmas 3, 4), and (4) All: E-STPM applied both pruning techniques.

Figs. 15, 16 show the results. It can be seen that (All)-E-STPM achieves the best performance among all versions. Its speedup w.r.t. (NoPrune)-E-STPM ranges from 3 up to 6 depending on the configurations, showing that the proposed prunings are very effective in improving E-STPM performance. Furthermore, (Trans)-E-STPM delivers larger speedup than (Apriori)-E-STPM. The average speedup is from 2 to 5 for (Trans)-E-STPM, and from 1.5 to 4 for (Apriori)-E-STPM. However, applying both always yields better speedup than applying either of them.

4) *Evaluation of A-STPM*: We proceed to evaluate the accuracy of A-STPM by comparing the patterns extracted by A-STPM and E-STPM. Table VII shows the accuracies of A-STPM for different $minSeason$ and $minDensity$ on the real-world datasets. It is seen that, A-STPM obtains high accuracy ($\geq 81\%$) when $minSeason$ and $minDensity$ are low, e.g., $minSeason = 8$ and $minDensity = 0.5\%$, and very high accuracy ($\geq 95\%$) when $minSeason$ and $minDensity$ are high, e.g., $minSeason = 16$ and $minDensity = 0.75\%$. Similarly, Table XII shows the accuracies of A-STPM on the synthetic datasets: very high accuracy ($\geq 96\%$) when $minSeason$ and $minDensity$ are high, e.g., $minSeason = 16$ and $minDensity = 0.75\%$.

VII. CONCLUSION AND FUTURE WORK

This paper presents our efficient Frequent Seasonal Temporal Pattern Mining from Time Series (FreqSTPfts) approach that offers: (1) the first solution for Seasonal Temporal Pattern Mining (STPM), (2) the efficient and exact Seasonal Temporal Pattern Mining (E-STPM) algorithm that employs the efficient data structures and pruning techniques to achieve fast mining, and (3) the approximate A-STPM that uses mutual information to prune unpromising time series and allows STPM to scale on big datasets. Extensive experiments conducted on real-world and synthetic datasets show that both A-STPM and E-STPM outperform the baseline, consume less memory, and scale well to big datasets. Compared to the baseline, the approximate A-STPM delivers up to an order of magnitude speedup. In future work, we plan to extend STPM to prune at the event level to further improve its performance.

REFERENCES

- [1] H. T. Lam, F. Mörchen, D. Fradkin, and T. Calders, "Mining compressing sequential patterns," *Statistical Analysis and Data Mining: The ASA Data Science Journal*, vol. 7, no. 1, pp. 34–52, 2014.
- [2] J.-W. Huang, C.-Y. Tseng, J.-C. Ou, and M.-S. Chen, "A general model for sequential pattern mining with a progressive database," *IEEE Transactions on knowledge and data engineering*, vol. 20, no. 9, pp. 1153–1167, 2008.
- [3] V. L. Ho, N. Ho, and T. B. Pedersen, "Efficient temporal pattern mining in big time series using mutual information," in *PVLDB*, vol. 15, no. 3, 2022.
- [4] Z. Lee, T. Lindgren, and P. Papapetrou, "Z-miner: an efficient method for mining frequent arrangements of event intervals," in *Proceedings of the 26th ACM SIGKDD International Conference on Knowledge Discovery & Data Mining*, 2020, pp. 524–534.
- [5] K. city infectious disease surveillance system. (2021) Kidss. [Online]. Available: <https://kidss.city.kawasaki.jp/>
- [6] O. Weather. (2021) Open weather. [Online]. Available: <https://openweathermap.org/>
- [7] R. U. Kiran, H. Shang, M. Toyoda, and M. Kitsuregawa, "Discovering recurring patterns in time series," in *EDBT*, 2015, pp. 97–108.
- [8] R. U. Kiran, C. Saideep, K. Zettsu, M. Toyoda, M. Kitsuregawa, and P. K. Reddy, "Discovering partial periodic spatial patterns in spatiotemporal databases," in *2019 IEEE International Conference on Big Data (Big Data)*. IEEE, 2019, pp. 233–238.
- [9] J. Han, W. Gong, and Y. Yin, "Mining segment-wise periodic patterns in time-related databases," in *KDD*, vol. 98, 1998, pp. 214–218.
- [10] J. Han, G. Dong, and Y. Yin, "Efficient mining of partial periodic patterns in time series database," in *Proceedings 15th International Conference on Data Engineering (Cat. No. 99CB36337)*. IEEE, 1999, pp. 106–115.
- [11] J. Assfalg, T. Bernecker, H.-P. Kriegel, P. Kröger, and M. Renz, "Periodic pattern analysis in time series databases," in *International Conference on Database Systems for Advanced Applications*. Springer, 2009, pp. 354–368.
- [12] M. Zhang, P. Wang, and W. Wang, "Efficient consensus motif discovery of all lengths in multiple time series," in *International Conference on Database Systems for Advanced Applications*. Springer, 2022, pp. 540–555.
- [13] H. Liu, F. Han, H. Zhou, X. Yan, and K. S. Kosik, "Fast motif discovery in short sequences," in *2016 IEEE 32nd International Conference on Data Engineering (ICDE)*. IEEE, 2016, pp. 1158–1169.
- [14] Y. Mohammad and T. Nishida, "Approximately recurring motif discovery using shift density estimation," in *International Conference on Industrial, Engineering and Other Applications of Applied Intelligent Systems*. Springer, 2013, pp. 141–150.
- [15] L. Kegel, C. Hartmann, M. Thiele, and W. Lehner, "Season-and trend-aware symbolic approximation for accurate and efficient time series matching," *Datenbank-Spektrum*, vol. 21, no. 3, pp. 225–236, 2021.
- [16] S. K. Tanbeer, C. F. Ahmed, B.-S. Jeong, and Y.-K. Lee, "Discovering periodic-frequent patterns in transactional databases," in *Pacific-Asia Conference on Knowledge Discovery and Data Mining*. Springer, 2009, pp. 242–253.
- [17] R. Uday Kiran and P. Krishna Reddy, "Towards efficient mining of periodic-frequent patterns in transactional databases," in *International Conference on Database and Expert Systems Applications*. Springer, 2010, pp. 194–208.
- [18] K. Amphawan, P. Lenca, and A. Surarerks, "Mining top-k periodic-frequent pattern from transactional databases without support threshold," in *International conference on advances in information technology*. Springer, 2009, pp. 18–29.
- [19] C. Cappiello, N. T. T. Ho, B. Pernici, P. Plebani, and M. Vitali, "Co 2-aware adaptation strategies for cloud applications," *IEEE Transactions on Cloud Computing*, vol. 4, no. 2, pp. 152–165, 2015.
- [20] T. T. N. Ho and B. Pernici, "A data-value-driven adaptation framework for energy efficiency for data intensive applications in clouds," in *2015 IEEE conference on technologies for sustainability (SusTech)*. IEEE, 2015, pp. 47–52.
- [21] A. Barkat, A. D. dos Santos, and T. T. N. Ho, "Open stack and cloud stack: Open source solutions for building public and private clouds," in *2014 16th International Symposium on Symbolic and Numeric Algorithms for Scientific Computing*. IEEE, 2014, pp. 429–436.
- [22] N. Ho, H. Vo, M. Vu, and T. B. Pedersen, "Amic: An adaptive information theoretic method to identify multi-scale temporal correlations in big time series data," *IEEE Transactions on Big Data*, vol. 7, no. 1, pp. 128–146, 2019.
- [23] N. Ho, H. Vo, and M. Vu, "An adaptive information-theoretic approach for identifying temporal correlations in big data sets," in *2016 IEEE International Conference on Big Data (Big Data)*. IEEE, 2016, pp. 666–675.
- [24] T. T. N. Ho, M. Gribaudo, and B. Pernici, "Characterizing energy per job in cloud applications," *Electronics*, vol. 5, no. 4, p. 90, 2016.
- [25] M. Gribaudo, T. T. N. Ho, B. Pernici, and G. Serazzi, "Analysis of the influence of application deployment on energy consumption," in *International Workshop on Energy Efficient Data Centers*. Springer, 2014, pp. 87–101.
- [26] N. Ho, T. B. Pedersen, M. Vu, C. A. Biscio *et al.*, "Efficient bottom-up discovery of multi-scale time series correlations using mutual information," in *2019 IEEE 35th International Conference on Data Engineering (ICDE)*. IEEE, 2019, pp. 1734–1737.
- [27] N. Ho, M. Gribaudo, and B. Pernici, "Improving energy efficiency for transactional workloads in cloud environments," in *Proceedings of the Eighth International Conference on Future Energy Systems*, 2017, pp. 290–295.
- [28] N. Ho, T. B. Pedersen, M. Vu *et al.*, "Efficient and distributed temporal pattern mining," in *2021 IEEE International Conference on Big Data (Big Data)*. IEEE, 2021, pp. 335–343.
- [29] V. L. Ho, N. Ho, and T. B. Pedersen, "Efficient temporal pattern mining in big time series using mutual information," *Proceedings of the VLDB Endowment*, vol. 15, no. 3, pp. 673–685, 2021.
- [30] N. Ho, V. L. Ho, T. B. Pedersen, M. Vu, and C. A. Biscio, "A unified approach for multi-scale synchronous correlation search in big time series—full version," *arXiv preprint arXiv:2204.09131*, 2022.
- [31] V. L. Ho, N. Ho, and T. B. Pedersen, "Efficient temporal pattern mining in big time series using mutual information—full version," *arXiv preprint arXiv:2010.03653*, 2020.
- [32] T. T. N. HO, "Towards sustainable solutions for applications in cloud computing and big data," in *Doctoral dissertation*. Politecnico di Milano, Italy, 2017, <http://hdl.handle.net/10589/131740>.
- [33] N. Ho, H. Vo, M. Vu, and T. B. Pedersen, "Amic: An adaptive information theoretic method to identify multi-scale temporal correlations in big time series data – accepted version," *arXiv preprint arXiv:1906.09995*, 2019.
- [34] T. T. N. HO, "Activity recognition using smartphone-based sensors," in *Master thesis*. Politecnico di Milano, Italy, 2013.
- [35] N. T. T. Ho, T. B. Pedersen, L. Van Ho, and M. Vu, "Efficient search for multi-scale time delay correlations in big time series," in *23rd International Conference on Extending Database Technology, EDBT 2020*. OpenProceedings.org, 2020, pp. 37–48.
- [36] P. Fournier-Viger, Y. Wang, P. Yang, J. C.-W. Lin, U. Yun, and R. U. Kiran, "Tspin: Mining top-k stable periodic patterns," *Applied Intelligence*, vol. 52, no. 6, pp. 6917–6938, 2022.
- [37] R. U. Kiran, Y. Watanobe, B. Chaudhury, K. Zettsu, M. Toyoda, and M. Kitsuregawa, "Discovering maximal periodic-frequent patterns in very large temporal databases," in *2020 IEEE 7th International Conference on Data Science and Advanced Analytics (DSAA)*. IEEE, 2020, pp. 11–20.
- [38] M. F. Javed, W. Nawaz, and K. U. Khan, "Hova-fppm: flexible periodic pattern mining in time series databases using hashed occurrence vectors and apriori approach," *Scientific Programming*, vol. 2021, 2021.
- [39] R. U. Kiran, M. Kitsuregawa, and P. K. Reddy, "Efficient discovery of periodic-frequent patterns in very large databases," *Journal of Systems and Software*, vol. 112, pp. 110–121, 2016.
- [40] R. U. Kiran, A. Anirudh, C. Saideep, M. Toyoda, P. K. Reddy, and M. Kitsuregawa, "Finding periodic-frequent patterns in temporal databases using periodic summaries," *Data Science and Pattern Recognition*, vol. 3, no. 2, pp. 24–46, 2019.
- [41] J. Lin, E. Keogh, S. Lonardi, and B. Chiu, "A symbolic representation of time series, with implications for streaming algorithms," in *Proceedings of the 8th ACM SIGMOD workshop on Research issues in data mining and knowledge discovery*, 2003, pp. 2–11.
- [42] J. F. Allen, "Maintaining knowledge about temporal intervals," *Communications of the ACM*, vol. 26, 1983.
- [43] V. L. Ho, N. Ho, and T. B. Pedersen, "Mining seasonal temporal patterns in time series," *arXiv preprint arXiv:2206.14604*, 2022. [Online]. Available: <https://arxiv.org/abs/2206.14604>

- [44] P. Papapetrou, G. Kollios, S. Sclaroff, and D. Gunopulos, "Mining frequent arrangements of temporal intervals," *KAIS*, vol. 21, 2009.
- [45] T. M. Cover and J. A. Thomas, *Elements of information theory*. John Wiley & Sons, 2012.
- [46] R. M. Corless, G. H. Gonnet, D. E. Hare, D. J. Jeffrey, and D. E. Knuth, "On the lambertw function," *Advances in Computational mathematics*, vol. 5, no. 1, pp. 329–359, 1996.
- [47] E.-E. T. Platform. (2019) Entso-e. [Online]. Available: <https://transparency.entsoe.eu/dashboard/show>
- [48] S. Moosavi, M. H. Samavatian, A. Nandi, S. Parthasarathy, and R. Ramnath, "Short and long-term pattern discovery over large-scale geo-spatiotemporal data," in *Proceedings of the 25th ACM SIGKDD International Conference on Knowledge Discovery & Data Mining*, 2019, pp. 2905–2913.

APPENDIX

A. Mutual exclusive property of temporal relations

Property 1. (Mutual exclusive) Consider the set of temporal relations $\mathfrak{R} = \{\text{Follows}, \text{Contains}, \text{Overlaps}\}$. Let E_i and E_j be two temporal events, and e_i occurring during $[t_{s_i}, t_{e_i}]$, e_j occurring during $[t_{s_j}, t_{e_j}]$ be their corresponding event instances, and ϵ be the tolerance buffer. The relations in \mathfrak{R} are mutually exclusive on E_i and E_j .

Proof. * **Case 1:** Assume the relation **Follows**($E_{i \triangleright e_i}, E_{j \triangleright e_j}$) holds between E_i and E_j . Thus, we have:

$$t_{e_i} \pm \epsilon \leq t_{s_j} \quad (12)$$

and:

$$t_{s_j} < t_{e_j} \Rightarrow t_{e_i} \pm \epsilon < t_{e_j} \quad (13)$$

Hence, **Contains**($E_{i \triangleright e_i}, E_{j \triangleright e_j}$) cannot exist between E_i and E_j , since **Contains**($E_{i \triangleright e_i}, E_{j \triangleright e_j}$) holds iff $(t_{s_i} \leq t_{s_j}) \wedge (t_{e_i} \pm \epsilon \geq t_{e_j})$ (contradict Eq. (13)). Similarly, **Overlaps**($E_{i \triangleright e_i}, E_{j \triangleright e_j}$) cannot exist between E_i and E_j since **Overlaps**($E_{i \triangleright e_i}, E_{j \triangleright e_j}$) holds iff $(t_{s_i} < t_{s_j}) \wedge (t_{e_i} \pm \epsilon < t_{e_j}) \wedge (t_{e_i} - t_{s_j} \geq d_o \pm \epsilon)$ (contradict Eq. (12)).

In conclusion, if **Follows**($E_{i \triangleright e_i}, E_{j \triangleright e_j}$) holds between E_i and E_j , then the two remaining relations cannot exist between E_i and E_j .

* **Case 2:** Assume the relation **Contains**($E_{i \triangleright e_i}, E_{j \triangleright e_j}$) holds between E_i and E_j . Thus, we have:

$$t_{s_i} \leq t_{s_j} \quad (14)$$

$$t_{e_i} \pm \epsilon \geq t_{e_j} \quad (15)$$

Hence, **Follows**($E_{i \triangleright e_i}, E_{j \triangleright e_j}$) cannot exist between E_i and E_j since **Follows**($E_{i \triangleright e_i}, E_{j \triangleright e_j}$) holds iff $t_{e_i} \pm \epsilon < t_{e_j}$ (contradict Eq. (15)).

Similarly, **Overlaps**($E_{i \triangleright e_i}, E_{j \triangleright e_j}$) cannot exist between E_i and E_j , since **Overlaps**($E_{i \triangleright e_i}, E_{j \triangleright e_j}$) holds iff $(t_{s_i} < t_{s_j}) \wedge (t_{e_i} \pm \epsilon < t_{e_j}) \wedge (t_{e_i} - t_{s_j} \geq d_o \pm \epsilon)$ (contradict Eq. (15)).

In conclusion, if **Contains**($E_{i \triangleright e_i}, E_{j \triangleright e_j}$) holds between E_i and E_j , then the two remaining relations cannot exist between E_i and E_j .

* **Case 3:** Assume the relation **Overlaps**($E_{i \triangleright e_i}, E_{j \triangleright e_j}$) holds between E_i and E_j . Thus, we have:

$$t_{s_i} < t_{s_j} \quad (16)$$

$$t_{e_i} \pm \epsilon < t_{e_j} \quad (17)$$

$$t_{e_i} - t_{s_j} \geq d_o \pm \epsilon \Rightarrow t_{s_j} \leq t_{e_i} - d_o \pm \epsilon \quad (18)$$

Hence, **Follows**($E_{i \triangleright e_i}, E_{j \triangleright e_j}$) cannot exist between E_i and E_j , since **Follows**($E_{i \triangleright e_i}, E_{j \triangleright e_j}$) holds iff $t_{e_i} \pm \epsilon < t_{s_j}$ (contradict Eq. (18)).

Similarly, **Contains**($E_{i \triangleright e_i}, E_{j \triangleright e_j}$) cannot exist between E_i and E_j , since **Contains**($E_{i \triangleright e_i}, E_{j \triangleright e_j}$) holds iff $t_{e_i} \pm \epsilon \geq t_{e_j}$ (contradict Eq. (17)).

In conclusion, if **Overlaps**($E_{i \triangleright e_i}, E_{j \triangleright e_j}$) holds between E_i and E_j , then the two remaining relations cannot exist between E_i and E_j . \square

B. Lemma 1

Lemma 1. Let P and P' be two temporal patterns such that $P' \subseteq P$. Then $\text{maxSeason}(P') \geq \text{maxSeason}(P)$.

Proof. We have:

$$\text{maxSeason}(P') = \frac{|SUP^{P'}|}{\text{minDensity}}, \text{maxSeason}(P) = \frac{|SUP^P|}{\text{minDensity}}$$

$$\text{Since: } |SUP^{P'}| \geq |SUP^P| \text{ (Derived from Def. 3.12)}$$

$$\text{Hence: } \text{maxSeason}(P') \geq \text{maxSeason}(P) \quad \square$$

C. Lemma 2

Lemma 2. Let P be a k -event temporal pattern formed by a k -event group (E_1, \dots, E_k) . Then, $\text{maxSeason}(P) \leq \text{maxSeason}(E_1, \dots, E_k)$.

Proof. Derived directly from Def. 3.12, and Eq. (1). \square

D. Mining frequent seasonal single event

Complexity: The complexity of finding frequent seasonal single events is $O(n \cdot |\mathcal{D}_{\text{SEQ}}|)$, where n is the number of distinct events.

Proof. Computing maxSeason for each event E_i takes $O(|\mathcal{D}_{\text{SEQ}}|)$. Thus, computing maxSeason for n events takes $O(n \cdot |\mathcal{D}_{\text{SEQ}}|)$. Moreover, for each candidate event E_i , identifying the set of seasons \mathcal{PS} takes $O(|SUP^{E_i}|)$. We have potentially n events. And thus, it takes $O(n \cdot |SUP^{E_i}|)$. The overall complexity is: $O(n \cdot |\mathcal{D}_{\text{SEQ}}| + n \cdot |SUP^{E_i}|) \sim O(n \cdot |\mathcal{D}_{\text{SEQ}}|)$. \square

E. Search space of STPM

Complexity: The search space of finding seasonal temporal patterns is $O(n^h 3^{h^2})$, where n is the number of distinct events in \mathcal{D}_{SEQ} , and h is the maximal length of a temporal pattern.

Proof. The number of seasonal single events is: $N_1 = n \sim O(n)$. For mining 2-event groups, the number of permutations of n distinct events taken 2 at a time is: $P(n, 2)$. However, since the same event can form a pair of events with itself, the total number of 2-event groups is: $N_2 = P(n, 2) + n \sim O(n^2)$. Each 2-event group in N_2 can form 3 different temporal relations, and thus, the total number of seasonal 2-event patterns is: $N_2 \times 3^1 \sim O(n^2 3^1)$. Similarly, the number of 3-event groups is: $N_3 = P(n, 3) + P(n, 2) + n \sim O(n^3)$, and the number of seasonal 3-event patterns is: $N_3 \times 3^3 \sim O(n^3 3^3)$. For mining h -event groups, the number of h -event groups is $O(n^h)$, while the number of seasonal h -event patterns is $O(n^h \times 3^{\frac{1}{2}h(h-1)}) \sim O(n^h 3^{h^2})$. Therefore, the total number of seasonal temporal patterns is $O(n) + O(n^2 3^1) + O(n^3 3^3) + \dots + O(n^h 3^{h^2}) \sim O(n^h 3^{h^2})$. \square

F. Lemma 3

Lemma 3. Let $S = \langle e_1, \dots, e_{k-1} \rangle$ be a temporal sequence, $P = \langle (r_{12}, E_{1 \triangleright e_1}, E_{2 \triangleright e_2}), \dots, (r_{(k-2)(k-1)}, E_{k-2 \triangleright e_{k-2}}, E_{k-1 \triangleright e_{k-1}}) \rangle$ be a $(k-1)$ -event pattern that occurs in S , e_k be a new event instance added to S to create the temporal sequence $S' = \langle e_1, \dots, e_k \rangle$. The set of temporal relations \mathfrak{R} is transitive on S' : $\forall e_i \in S', i < k, \exists r \in \mathfrak{R}$ s.t. $r(E_{i \triangleright e_i}, E_{k \triangleright e_k})$ hold.

Proof. Since $S' = \langle e_1, \dots, e_n \rangle$ is a temporal sequence, the event instances in S' are chronologically ordered by their start times. Then, $\forall e_i \in S', i \neq n: t_{s_i} \leq t_{s_n}$. We have:

- If $t_{e_i} \pm \epsilon \leq t_{s_n}$, then $E_{i_{\triangleright e_i}} \rightarrow E_{n_{\triangleright e_n}}$.
- If $(t_{s_i} \leq t_{s_n}) \wedge (t_{e_i} \pm \epsilon \geq t_{e_n})$, then $E_{i_{\triangleright e_i}} \succcurlyeq E_{n_{\triangleright e_n}}$.
- If $(t_{s_i} < t_{s_n}) \wedge (t_{e_i} \pm \epsilon < t_{e_n}) \wedge (t_{e_i} - t_{s_n} \geq d_o \pm \epsilon)$ where d_o is the minimal overlapping duration, then $E_{i_{\triangleright e_i}} \not\subseteq E_{n_{\triangleright e_n}}$.

□

G. Lemma 4

Lemma 4. Let $N_{k-1} = (E_1, \dots, E_{k-1})$ be a candidate seasonal $(k-1)$ -event group, and E_k be a candidate seasonal single event. The group $N_k = N_{k-1} \cup E_k$ can form candidate seasonal k -event temporal patterns if $\forall E_i \in N_{k-1}, \exists r \in \mathcal{R}$ s.t. $r(E_i, E_k)$ is a candidate seasonal temporal relation.

Proof. Let p_k be any k -event pattern formed by N_k . Then p_k is a list of $\frac{1}{2}k(k-1)$ triples (E_i, r_{ij}, E_j) where each represents a relation $r(E_i, E_j)$ between two events. In order for p_k to be a candidate seasonal k -event temporal pattern, each of the relations in p_k must be a candidate seasonal temporal pattern (Def. 3.8, Eq. (1), and Lemmas 1 and 3). □

H. Mining frequent seasonal k -event pattern

Complexity: Let n be the number of single events in HLH_1 , i be the average number of event instances of each event, r be the number of $(k-1)$ -event patterns in HLH_{k-1} , and u be the average number of granules of each event/temporal relation. The complexity of frequent seasonal k -event pattern mining is $O(n^2 i^2 u^2) + O(|F_1| \cdot |F_{k-1}| \cdot r \cdot k^2 \cdot u)$.

*Proof. * The complexity of frequent seasonal 2-event pattern mining:* The Cartesian product of n events in HLH_1 generates n^2 2-event groups. Computing $maxSeason$ of n^2 2-event groups takes $O(n^2 u)$. For each 2-event group, we need to compute $maxSeason$ of their temporal relations, which takes $O(i^2 u^2)$. We have potentially n^2 nodes. And thus, it takes $O(n^2 i^2 u^2)$. For each candidate 2-event pattern, identifying the set of season \mathcal{PS} takes $O(u)$. And we have potentially $(3n^2)$ relations. Thus, finding \mathcal{PS} takes $O(3n^2 u) \sim O(n^2 u)$. The complexity of frequent seasonal 2-event pattern mining is: $O(n^2 u + n^2 i^2 u^2) \sim O(n^2 i^2 u^2)$.

** The complexity of frequent seasonal k -event pattern mining ($k > 2$):* For each $(k-1)$ -event pattern, we need to compute the support set of $\frac{1}{2}(k-1)(k-2)$ triples, which takes $O(\frac{1}{2}(k-1)(k-2)u) \sim O(k^2 u)$. We have $|F_1| \times |F_{k-1}|$ events, each has r $(k-1)$ -event patterns. Thus, the complexity of computing $maxSeason$ is $O(|F_1| \cdot |F_{k-1}| \cdot r \cdot k^2 \cdot u)$. For each candidate pattern, identifying its \mathcal{PS} takes $O(u)$. We have potentially $|F_1| \times |F_{k-1}| \times r$ patterns. Thus, it takes $O(|F_1| \cdot |F_{k-1}| \cdot r \cdot u)$. The complexity of frequent seasonal k -event pattern mining ($k > 2$) is: $O(|F_1| \cdot |F_{k-1}| \cdot r \cdot k^2 \cdot u + |F_1| \cdot |F_{k-1}| \cdot r \cdot u) \sim O(|F_1| \cdot |F_{k-1}| \cdot r \cdot k^2 \cdot u)$.

Thus, the total complexity is $O(n^2 i^2 u^2) + O(|F_1| \cdot |F_{k-1}| \cdot r \cdot k^2 \cdot u)$. □

I. Theorem

Theorem 1. (Lower bound of the maximum seasonal occurrence) Let μ be the mutual information threshold. If the NMI $\tilde{I}(X_S; Y_S) \geq \mu$, then the maximum seasonal occurrence of (X_1, Y_1) in \mathcal{D}_{SEQ} has a lower bound:

$$maxSeason(X_1, Y_1) \geq \frac{\lambda_2 \cdot |\mathcal{D}_{SEQ}|}{minDensity} \cdot e^{W\left(\frac{\log \lambda_1^{1-\mu} \cdot \ln 2}{\lambda_2}\right)} \quad (19)$$

where: $\lambda_1 = \min\{p(X_i), \forall X_i \in X_S\}$ is the minimum probability of $X_i \in X_S$, and $\lambda_2 = p(Y_1)$ is the probability of $Y_1 \in Y_S$, and W is the Lambert function [46].

Proof. From Eq. (5), we have:

$$\tilde{I}(X_S; Y_S) = 1 - \frac{H(X_S|Y_S)}{H(X_S)} \geq \mu \quad (20)$$

Hence:

$$\frac{H(X_S|Y_S)}{H(X_S)} \leq 1 - \mu \quad (21)$$

First, we derive a lower bound for $\frac{H(X_S|Y_S)}{H(X_S)}$. We have:

$$\begin{aligned} \frac{H(X_S|Y_S)}{H(X_S)} &= \frac{p(X_1, Y_1) \cdot \log \frac{p(X_1, Y_1)}{p(Y_1)}}{\sum_i p(X_i) \cdot \log p(X_i)} \\ &+ \frac{\sum_{i \neq 1 \& j \neq 1} p(X_i, Y_j) \cdot \log \frac{p(X_i, Y_j)}{p(Y_j)}}{\sum_i p(X_i) \cdot \log p(X_i)} \end{aligned} \quad (22)$$

We first consider the numerator in Eq. (22), we have:

$$\begin{aligned} p(X_1, Y_1) \cdot \log \frac{p(X_1, Y_1)}{p(Y_1)} &+ \sum_{i \neq 1 \& j \neq 1} p(X_i, Y_j) \cdot \log \frac{p(X_i, Y_j)}{p(Y_j)} \\ &\leq p(X_1, Y_1) \cdot \log \frac{p(X_1, Y_1)}{p(Y_1)} \\ &\leq p(X_1, Y_1) \cdot \log \frac{p(X_1, Y_1)}{\lambda_2} \end{aligned} \quad (23)$$

where $\lambda_2 = p(Y_1)$.

Next, we consider the denominator in Eq. (22). Suppose that:

$$p(X_k) = \min\{p(X_i)\}, \forall X_i \in X_S \quad (24)$$

Then we have:

$$\begin{aligned} p(X_i) &\geq p(X_k), \forall X_i \in X_S \\ &\Rightarrow \log p(X_i) \geq \log p(X_k) \\ &\Rightarrow p(X_i) \log p(X_i) \geq p(X_i) \log p(X_k) \\ &\Rightarrow \sum_i p(X_i) \log p(X_i) \geq \sum_i p(X_i) \log p(X_k) \\ &= \log p(X_k) \sum_i p(X_i) \\ &= \log p(X_k) \\ &= \log \lambda_1 \end{aligned} \quad (25)$$

where $\lambda_1 = p(X_k)$.

Replace Eqs. (23) and (25) into Eq. (22), we get:

$$\frac{H(X_S|Y_S)}{H(X_S)} \geq \frac{p(X_1, Y_1) \cdot \log \frac{p(X_1, Y_1)}{\lambda_2}}{\log \lambda_1} \quad (26)$$

From Eqs. (21) and (26), it follows that:

$$(1 - \mu) \geq \frac{p(X_1, Y_1) \cdot \log \frac{p(X_1, Y_1)}{\lambda_2}}{\log \lambda_1}$$

$$\Leftrightarrow p(X_1, Y_1) \cdot \log \frac{p(X_1, Y_1)}{\lambda_2} \geq \log \lambda_1^{1-\mu} \quad (27)$$

Assign $x = p(X_1, Y_1)$, $b = \log \lambda_1^{1-\mu}$. Replace x and b into Eq. (27), we get:

$$x \cdot \log \frac{x}{\lambda_2} \geq b$$

$$\Leftrightarrow \frac{x}{\lambda_2} \cdot \log \frac{x}{\lambda_2} \geq \frac{b}{\lambda_2}$$

$$\Leftrightarrow \frac{x}{\lambda_2} \cdot \frac{\ln \frac{x}{\lambda_2}}{\ln 2} \geq \frac{b}{\lambda_2}$$

$$\Leftrightarrow \frac{x}{\lambda_2} \cdot \ln \frac{x}{\lambda_2} \geq \frac{b \cdot \ln 2}{\lambda_2} \quad (28)$$

Assign $y = \ln \frac{x}{\lambda_2} \Rightarrow \frac{x}{\lambda_2} = e^y$. Replace y and e^y into Eq. (28), we get:

$$y \cdot e^y \geq \frac{b \cdot \ln 2}{\lambda_2}$$

$$\Leftrightarrow y \geq W\left(\frac{b \cdot \ln 2}{\lambda_2}\right), \text{ where } W \text{ is the Lambert function [46].}$$

$$\Leftrightarrow \ln \frac{x}{\lambda_2} \geq W\left(\frac{\log \lambda_1^{1-\mu} \cdot \ln 2}{\lambda_2}\right)$$

$$\Leftrightarrow e^{\ln \frac{x}{\lambda_2}} \geq e^{W\left(\frac{\log \lambda_1^{1-\mu} \cdot \ln 2}{\lambda_2}\right)}$$

$$\Leftrightarrow \frac{x}{\lambda_2} \geq e^{W\left(\frac{\log \lambda_1^{1-\mu} \cdot \ln 2}{\lambda_2}\right)}$$

$$\Leftrightarrow x \geq \lambda_2 \cdot e^{W\left(\frac{\log \lambda_1^{1-\mu} \cdot \ln 2}{\lambda_2}\right)}$$

$$\Leftrightarrow p(X_1, Y_1) \geq \lambda_2 \cdot e^{W\left(\frac{\log \lambda_1^{1-\mu} \cdot \ln 2}{\lambda_2}\right)} \quad (29)$$

Since the relative support of (X_1, Y_1) in \mathcal{D}_{SEQ} is greater than or equal to the relative support of (X_1, Y_1) in \mathcal{D}_{SYB} [3], hence:

$$\frac{|SUP^{(X_1, Y_1)}|}{|\mathcal{D}_{\text{SEQ}}|} \geq \frac{|SUP_{\mathcal{D}_{\text{SYB}}}^{(X_1, Y_1)}|}{|\mathcal{D}_{\text{SYB}}|} = p(X_1, Y_1) \quad (30)$$

where $\frac{|SUP_{\mathcal{D}_{\text{SYB}}}^{(X_1, Y_1)}|}{|\mathcal{D}_{\text{SYB}}|}$ is the relative support of (X_1, Y_1) in \mathcal{D}_{SYB} .

From Eqs. (29) and (30), it follows that:

$$\frac{|SUP^{(X_1, Y_1)}|}{|\mathcal{D}_{\text{SEQ}}|} \geq \lambda_2 \cdot e^{W\left(\frac{\log \lambda_1^{1-\mu} \cdot \ln 2}{\lambda_2}\right)}$$

$$\Leftrightarrow \frac{|SUP^{(X_1, Y_1)}|}{\minDensity} \geq \frac{\lambda_2 \cdot |\mathcal{D}_{\text{SEQ}}|}{\minDensity} \cdot e^{W\left(\frac{\log \lambda_1^{1-\mu} \cdot \ln 2}{\lambda_2}\right)}$$

$$\Leftrightarrow \maxSeason(X_1, Y_1) \geq \frac{\lambda_2 \cdot |\mathcal{D}_{\text{SEQ}}|}{\minDensity} \cdot e^{W\left(\frac{\log \lambda_1^{1-\mu} \cdot \ln 2}{\lambda_2}\right)} \quad (31)$$

We can derive a lower bound of μ from Eq. (31).

$$\maxSeason(X_1, Y_1) \geq \frac{\lambda_2 \cdot |\mathcal{D}_{\text{SEQ}}|}{\minDensity} \cdot e^{W\left(\frac{\log \lambda_1^{1-\mu} \cdot \ln 2}{\lambda_2}\right)} \geq \minSeason$$

$$\Rightarrow e^{W\left(\frac{\log \lambda_1^{1-\mu} \cdot \ln 2}{\lambda_2}\right)} \geq \frac{\minSeason \cdot \minDensity}{\lambda_2 \cdot |\mathcal{D}_{\text{SEQ}}|}$$

$$\Leftrightarrow e^{W\left(\frac{\log \lambda_1^{1-\mu} \cdot \ln 2}{\lambda_2}\right)} \geq \rho \quad (32)$$

where $\rho = \frac{\minSeason \cdot \minDensity}{\lambda_2 \cdot |\mathcal{D}_{\text{SEQ}}|}$.

To solve Eq. (32), we consider two cases.

* **Case 1:** $0 \leq \rho \leq \frac{1}{e}$, we have:

$$\frac{\log \lambda_1^{1-\mu} \cdot \ln 2}{\lambda_2} \geq \frac{-1}{e}$$

$$\Leftrightarrow \log \lambda_1^{1-\mu} \geq \frac{-\lambda_2}{e \cdot \ln 2}$$

$$\Leftrightarrow (1 - \mu) \cdot \log \lambda_1 \geq \frac{-\lambda_2}{e \cdot \ln 2}$$

$$\Leftrightarrow 1 - \mu \leq \frac{-\lambda_2}{e \cdot \ln 2 \cdot \log \lambda_1} \quad (\log \lambda_1 < 0)$$

$$\Leftrightarrow \mu \geq 1 + \frac{\lambda_2}{e \cdot \ln 2 \cdot \log \lambda_1}$$

$$\Leftrightarrow \mu \geq 1 - \frac{\lambda_2}{e \cdot \ln 2 \cdot \log \frac{1}{\lambda_1}} \quad (33)$$

* **Case 2:** $\rho > \frac{1}{e}$, we have:

$$\frac{\log \lambda_1^{1-\mu} \cdot \ln 2}{\lambda_2} \geq \rho \cdot \log \rho$$

$$\Leftrightarrow \log \lambda_1^{1-\mu} \geq \rho \cdot \lambda_2 \cdot \frac{\log \rho}{\ln 2}$$

$$\Leftrightarrow (1 - \mu) \cdot \log \lambda_1 \geq \rho \cdot \lambda_2 \cdot \frac{\log \rho}{\ln 2}$$

$$\Leftrightarrow 1 - \mu \leq \rho \cdot \lambda_2 \cdot \frac{\log \rho}{\ln 2 \cdot \log \lambda_1} \quad (\log \lambda_1 < 0)$$

$$\Leftrightarrow \mu \geq 1 - \frac{\rho \cdot \lambda_2 \cdot \log \rho}{\ln 2 \cdot \log \lambda_1} \quad (34)$$

□

J. Qualitative Evaluation

Tables XIII and XIV list the number of seasonal patterns found in the SC and HFM datasets. It can be seen that high *minSeason* leads to less generated patterns, as many have few seasonal occurrences. Moreover, high *minDensity* also generates fewer patterns since only few patterns have high occurrence density. Finally, high *maxPeriod* results in more generated patterns, since high *maxPeriod* allows more temporal relations to be formed, thus increasing the number of patterns.

TABLE XIII: The Number of Seasonal Patterns on SC

maxPeriod (%)	minSeason (#) · minDensity (%)								
	8-0.5	8-0.75	8-1.0	12-0.5	12-0.75	12-1.0	16-0.5	16-0.75	16-1.0
0.2	17241	12401	8632	10973	8291	3742	6207	3416	2138
0.4	24948	18293	11827	16830	12726	5291	8263	5084	3816
0.6	31825	26108	14039	24806	19408	8032	11852	8165	6010

TABLE XIV: The Number of Seasonal Patterns on HFM

maxPeriod (%)	minSeason (#) - minDensity (%)								
	8-0.5	8-0.75	8-1.0	12-0.5	12-0.75	12-1.0	16-0.5	16-0.75	16-1.0
0.2	14763	10425	7191	8014	7125	2486	4452	2693	1307
0.4	19542	14018	8506	11036	9082	5563	6207	5261	3005
0.6	22671	17039	10617	13502	10539	8035	7658	7014	4092

K. Baselines comparison

Figs. 17, 18, 19, and 20 show the experimental results on SC and HFM datasets. Note that Figs. 17-24 use the same legend.

As shown in Figs. 17 and 18, A-STPM achieves the best runtime among all methods, and E-STPM has better runtime than the baseline. The range and average speedups of A-STPM compared to other methods are: [1.4-3.1] and 2.2 (E-STPM), and [4.9-10.3] and 6.9 (APS-growth). The speedup of E-STPM compared to the baseline is [2.8-5.4] and 3.5 on average. Note that the time to compute MI and μ for SC and HFM in Figs. 17 and 18 are 0.9 and 1.2 seconds, respectively.

In terms of memory consumption, as shown in Figs. 19 and 20, A-STPM is the most efficient method, while E-STPM is more efficient than the baseline. The range and the average memory consumption of A-STPM compared to other methods are: [1.4-2.6] and 1.7 (E-STPM), and [2.5-6.3] and 3.7 (APS-growth). The memory usage of E-STPM compared to the baseline is [1.3-3.2] and 2.1 on average.

L. Scalability evaluation on synthetic datasets

Figs. 21 and 22 show the runtimes of A-STPM, E-STPM and the baseline when the number of sequences changes. We obtain the range and average speedups of A-STPM are: [1.4-2.7] and 2.1 (E-STPM), and [2.4-6.1] and 4.2 (APS-growth). Similarly, the range and average speedup of E-STPM compared to APS-growth is [1.6-3.5] and 2.8. We note that the baseline fails for larger configurations in this scalability study, i.e., on the synthetic SC at 60% sequences (Fig. 21a) and on the synthetic HFM at 100% sequences (Fig. 22a), showing that A-STPM and E-STPM can scale well on big datasets while the baseline cannot.

Figs. 23 and 24 compare the runtimes of A-STPM, E-STPM and APS-growth when changing the number of time series. We obtain the range and average speedups of A-STPM are: [1.4-2.9] and 2.2 (E-STPM), and [3.1-6.7] and 4.5 (APS-growth), and of E-STPM is [1.7-3.8] and 2.9 (APS-growth). The baseline also fails at large configurations in this study, i.e., when # Time Series ≥ 6000 on the synthetic SC (Fig. 23a) and the synthetic HFM (Fig. 24a).

Finally, we provide the percentage of time series and events pruned by A-STPM in the scalability test in Tables XV and XVI. Here, we can see that low *minSeason* and *minDensity* lead to more time series (events) to be pruned because low *minSeason* and *minDensity* result in higher μ .

M. Evaluation of the pruning techniques in E-STPM

In this section, we report the evaluation results of the proposed pruning techniques in E-STPM on SC and HFM. We use 3 different configurations that vary: the minimum season, the minimum density, and the maximum period. Figs. 25 and

TABLE XV: Pruned Time Series and Events from A-STPM on SC

# Attr.	# Pruned Time Series			# Pruned Events		
	12-0.5%	16-0.75%	20-1.0%	12-0.5%	16-0.75%	20-1.0%
2000	31.60	29.20	25.30	30.23	26.26	20.04
4000	30.10	26.05	18.45	29.01	25.66	19.90
6000	28.35	24.22	18.25	28.83	25.02	19.83
8000	26.78	24.05	17.80	28.79	24.64	19.49
10000	26.03	23.01	17.49	25.19	22.53	18.13

TABLE XVI: Pruned Time Series and Events from A-STPM on HFM

# Attr.	# Pruned Time Series			# Pruned Events		
	12-0.5%	16-0.75%	20-1.0%	12-0.5%	16-0.75%	20-1.0%
2000	38.10	31.35	28.90	27.46	24.68	20.72
4000	32.65	29.58	22.60	26.22	24.58	20.29
6000	31.12	27.85	20.28	25.41	23.78	19.84
8000	29.33	27.15	20.08	24.83	23.21	19.17
10000	28.84	25.09	19.68	24.54	23.01	18.97

26 show the results. It can be seen that All-E-STPM achieves the best performance among all versions. Its speedup w.r.t. NoPrune-E-STPM ranges from 2.5 up to 4.5 depending on the configurations, showing that the proposed prunings are very effective in improving E-STPM performance. The average speedup is from 2 to 4 for Trans-E-STPM, and from 1.5 to 3 for Apriori-E-STPM. However, applying both always yields better speedup than applying either of them.

N. Evaluation of A-STPM

Table XVII shows the accuracies of A-STPM for different *minSeason* and *minDensity* on the real world datasets. It is seen that, A-STPM obtains high accuracy ($\geq 80\%$) when *minSeason* and *minDensity* are low, e.g., *minSeason* = 8 and *minDensity* = 0.5%, and very high accuracy ($\geq 95\%$) when *minSeason* and *minDensity* are high, e.g., *minSeason* = 16 and *minDensity* = 0.75%. Similarly, Table XVIII shows the accuracies of A-STPM on the synthetic datasets: very high accuracy ($\geq 95\%$) when *minSeason* and *minDensity* are high, e.g., *minSeason* = 16 and *minDensity* = 0.75%.

TABLE XVII: A-STPM Accuracy

# minSeason	minDensity (%)					
	SC (real)			HFM (real)		
	0.5	0.75	1	0.5	0.75	1
8	80	81	87	82	84	89
12	83	85	93	86	92	94
16	92	95	100	96	97	100
20	95	99	100	97	100	100

TABLE XVIII: The Accuracy of A-STPM on Syn. Data

# Attr.	SC			HFM		
	Accuracy (%)			Accuracy (%)		
	12-0.5%	16-0.75%	20-1.0%	12-0.5%	16-0.75%	20-1.0%
2000	84	95	100	87	98	100
4000	85	96	100	87	98	100
6000	85	97	100	90	98	100
8000	87	97	100	93	98	100
10000	88	98	100	94	99	100

O. Evaluation of the tolerance buffer ϵ

We evaluate the impact of the buffer ϵ on extracted seasonal patterns. Tables XIX and XX report the number of extracted seasonal patterns for different ϵ values, and the corresponding percentages of pattern loss compared to $\epsilon = 0$. For RE and SC datasets, there are no lost patterns with $\epsilon = 1$ hour. For INF and HFM datasets, there are no lost patterns with $\epsilon = 1$ day and $\epsilon = 2$ days. And the losses among other ϵ values are very low since there is low noise level in the datasets.

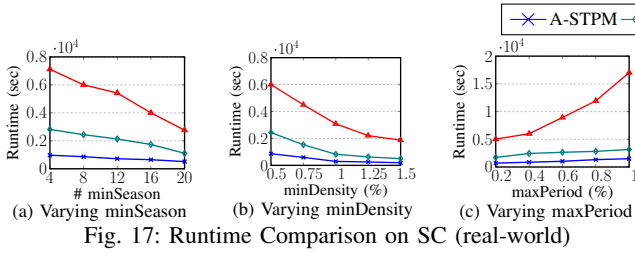


Fig. 17: Runtime Comparison on SC (real-world)

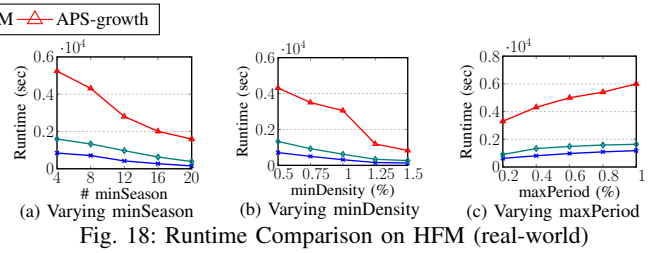


Fig. 18: Runtime Comparison on HFM (real-world)

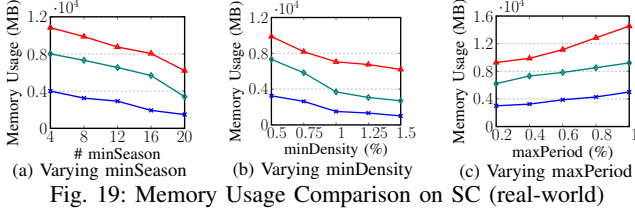


Fig. 19: Memory Usage Comparison on SC (real-world)

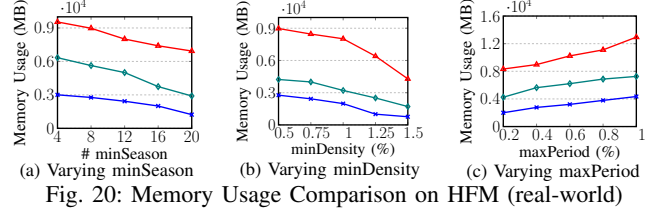


Fig. 20: Memory Usage Comparison on HFM (real-world)

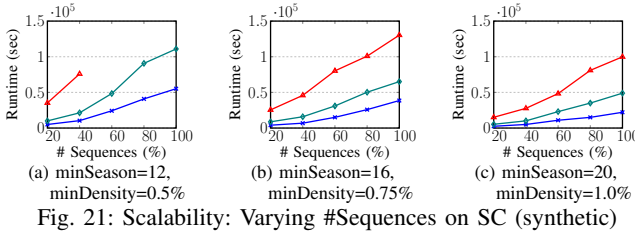


Fig. 21: Scalability: Varying #Sequences on SC (synthetic)

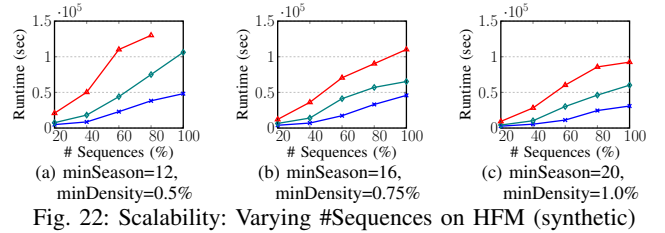


Fig. 22: Scalability: Varying #Sequences on HFM (synthetic)

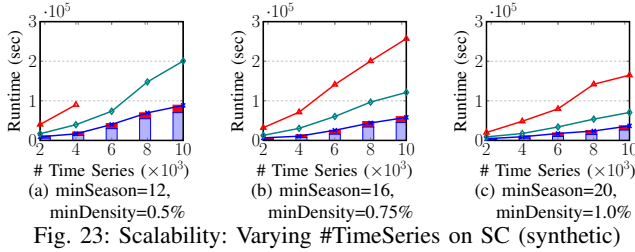


Fig. 23: Scalability: Varying #TimeSeries on SC (synthetic)

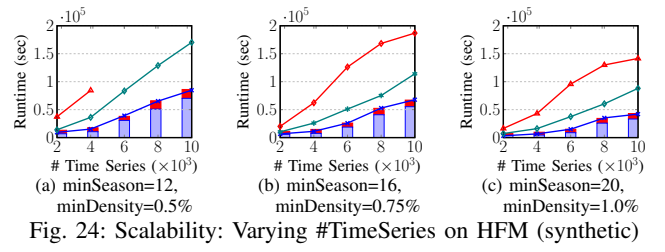


Fig. 24: Scalability: Varying #TimeSeries on HFM (synthetic)

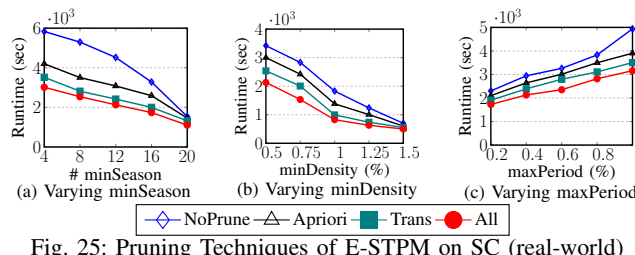


Fig. 25: Pruning Techniques of E-STPM on SC (real-world)

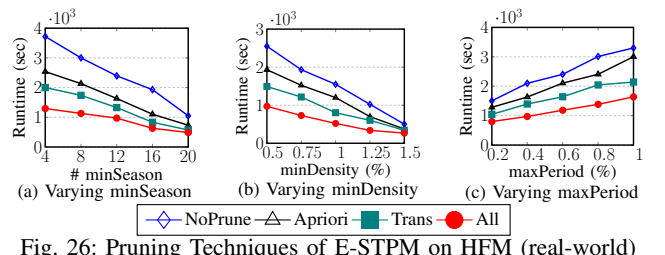


Fig. 26: Pruning Techniques of E-STPM on HFM (real-world)

TABLE XIX: Number of Extracted Patterns and Percentages of Pattern Loss on RE and SC

ϵ value	RE		SC	
	# Patterns	Patterns (%)	# Patterns	Patterns (%)
1 hour	35626	0.00	17241	0.00
2 hours	35407	0.61	16921	1.85
3 hours	35192	1.21	16812	2.48

TABLE XX: Number of Extracted Patterns and Percentages of Pattern Loss on INF and HFM

ϵ value	INF		HFM	
	# Patterns	Patterns (%)	# Patterns	Patterns (%)
1 day	7812	0.00	14763	0.00
2 days	7812	0.00	14763	0.00
3 days	7803	0.11	14750	0.08